A 3D brain unit model to further improve prediction of local drug distribution within the brain

Vendel, E.; Rottschäfer, V.; Lange, E.C.M. de

PLOS ONE

RESEARCH ARTICLE

A 3D brain unit model to further improve prediction of local drug distribution within the brain

Esmée Vendel[1], **Vivi Rottschäfer**[1]*, **Elizabeth C. M. de Lange**[2]*

1 Mathematical Institute, Leiden University, Leiden, The Netherlands, **2** Leiden Academic Centre for Drug Research, Leiden University, Leiden, The Netherlands

* vivi@math.leidenuniv.nl (VR); ecmdelange@lacdr.leidenuniv.nl (EL)

Abstract

The development of drugs targeting the brain still faces a high failure rate. One of the reasons is a lack of quantitative understanding of the complex processes that govern the pharmacokinetics (PK) of a drug within the brain. While a number of models on drug distribution into and within the brain is available, none of these addresses the combination of factors that affect local drug concentrations in brain extracellular fluid (brain ECF). Here, we develop a 3D brain unit model, which builds on our previous proof-of-concept 2D brain unit model, to understand the factors that govern local unbound and bound drug PK within the brain. The 3D brain unit is a cube, in which the brain capillaries surround the brain ECF. Drug concentration-time profiles are described in both a blood-plasma-domain and a brain-ECF-domain by a set of differential equations. The model includes descriptions of blood plasma PK, transport through the blood-brain barrier (BBB), by passive transport via paracellular and transcellular routes, and by active transport, and drug binding kinetics. The impact of all these factors on ultimate local brain ECF unbound and bound drug concentrations is assessed. In this article we show that all the above mentioned factors affect brain ECF PK in an interdependent manner. This indicates that for a quantitative understanding of local drug concentrations within the brain ECF, interdependencies of all transport and binding processes should be understood. To that end, the 3D brain unit model is an excellent tool, and can be used to build a larger network of 3D brain units, in which the properties for each unit can be defined independently to reflect local differences in characteristics of the brain.

Citation: Vendel E, Rottschäfer V, de Lange ECM (2020) A 3D brain unit model to further improve prediction of local drug distribution within the brain. PLoS ONE 15(9): e0238397. https://doi.org/10.1371/journal.pone.0238397

Editor: Stefan Liebner, Institute of Neurology (Edinger-Institute), GERMANY

Received: March 20, 2020

Accepted: August 15, 2020

Published: September 23, 2020

Data Availability Statement: All relevant data are within the manuscript.

Funding: The authors received no specific funding for this work.

Competing interests: The authors have declared that no competing interests exist.

1 Introduction

The brain capillary bed is the major site of drug exchange between the blood and the brain. Blood flows from the general blood circulation into the brain capillary bed by a feeding arteriole and back by a draining venule. The rate at which drug molecules within the blood are exposed to the brain is determined by the brain capillary blood flow rate. Drug exchange between the blood plasma in the brain capillaries and the brain extracellular fluid (ECF) is controlled by the blood-brain barrier (BBB).

Drug distribution into and within the brain has been extensively summarized in a recent review [1]. In short, the BBB has great impact on the relationship between the concentration-time profiles of unbound drug in the blood plasma (blood plasma pharmacokinetics (PK)) and in the brain ECF (brain ECF PK). The BBB consists of brain endothelial cells that are held closely together by tight junctions. Unbound drug may cross the BBB by passive and/or active transport [2–10]. Passive transport is bidirectional and occurs by diffusion through the BBB endothelial cells (transcellular transport) and through the BBB tight junctions between the endothelial cells (paracellular transport). Passive transport is quantified by the BBB permeability, which is the speed by which a compound passively crosses the BBB, and depends on the properties of both the drug and the brain. Active transporters located at the BBB move compounds either inward (in the direction of the brain ECF, active efflux) or outward (in the direction of the blood plasma, active efflux). Once having crossed the BBB, drug distributes within the brain ECF by diffusion. Diffusion within the brain ECF is hindered by the brain cells [11, 12]. This hindrance is described by the so-called tortuosity and leads to an effective diffusion that is smaller than normal (in a medium without obstacles). Moreover, a fluid flow, the brain ECF bulk flow, is present. The brain ECF bulk flow results from the generation of brain ECF by the BBB and drainage into the cerebrospinal fluid (CSF). Both diffusion and brain ECF bulk flow are important for the distribution of a drug to its target site, which is the site where a drug exerts its effect. In order to do induce an effect, a drug needs to bind to specific binding sites (targets). Only unbound drug, i.e. drug that is not bound to any components of the brain, can interact with its target [13, 14]. This is a dynamic process of association and dissociation, the so-called drug binding kinetics. These association and dissociation rates may affect the concentration of unbound drug at the target site [15, 16]. While the drug dissociation rate has been thought of as the most important determinant of the duration of interactions between a drug and its binding site [17], a more recent study shows that the drug association rate is equally important [16].

A number of models integrating several of the discussed processes of drug distribution into and within the brain is available, see for example [11, 12, 18–25] and [26]. The most recent and comprehensive brain drug distribution model is the physiologically-based pharmacokinetic model for the rat and for human [27, 28]. This model takes multiple compartments of the central nervous system (CNS) into account, including plasma PK, passive paracellular and transcellular BBB transport, active BBB transport, and distribution between the brain ECF, intracellular spaces, and multiple CSF sites, on the basis of CNS-specific and drug-specific parameters. However, it does not take into account distribution within brain tissue (brain ECF).

Much is still unknown on the spatial distribution of a drug within the brain and quantitative data on the processes governing brain spatial-temporal drug transport are lacking. The purpose of the present study is therefore to gain insight into the processes governing spatial drug distribution within the brain. Here, we developed a 3D brain unit model, in which local brain drug distribution is explicitly taken into account. The 3D brain unit model encompasses blood plasma PK, the BBB, brain ECF, brain ECF bulk flow, diffusion, and binding to specific and non-specific binding sites [29, 30] within the brain. This 3D piece of brain tissue can be considered the smallest physiological unit of the brain in terms of drug transport. Within the 3D brain unit, drug is carried along with the blood plasma by the brain capillary blood flow and as such presented to the brain ECF. Drug distributes between the blood plasma and the brain ECF by transport across the BBB. Thereafter, drug distribution within the brain ECF is affected by diffusion, bulk flow and binding. We describe the distribution of drug within the brain ECF by a partial differential equation (PDE) and couple this to two ordinary differential equations (ODEs) to account for specific and non-specific drug binding.

The model builds on a proof-of-concept 2D brain unit model [31]. The 2D model is a basic model covering many essential aspects of drug distribution within the brain, including passive BBB transport, diffusion, brain ECF bulk flow, specific binding of a drug at its target site and non-specific binding of a drug to components of the brain. Here, brain cells are implicitly implemented by describing the hindrance the cells impose on the transport of a drug within the brain ECF in a tortuosity term, λ. There, λ is defined as $\sqrt{\frac{D}{D^*}}$, with D being the normal diffusion coefficient and D^* the effective diffusion coefficient [12]. The 2D brain unit model has enabled the study of the effect of drug properties and brain tissue characteristics on the distribution of a drug within the brain ECF and on its specific and non-specific binding behaviour of the drug.

The current *3D* brain unit model further improves the prediction of drug distribution within the brain. The third dimension improves the realistic features of the model as the brain is also 3D. Moreover, the third dimension allows the brain ECF to be not entirely surrounded by capillaries, such that the brain ECF is a continuous medium, like in reality. Then, the brain capillary blood flow and active transport across the BBB, which are both important mechanisms of drug transport into the brain, are included. Here, we focus on one single brain unit. This allows for a thorough characterisation of drug distribution within one 3D brain unit before expanding to a larger scale.

In the remainder of this article, the mathematical representation of the characteristics of the 3D brain unit is introduced (section 2). There, we formulate the model (section 2.1) and the mathematical descriptions of the drug distribution within the blood plasma of the brain capillaries (section 2.2) and within the brain (section 2.3). In section 2.4 we formulate the model boundary conditions that describe drug exchange between the blood plasma and the brain ECF by passive and active BBB transport, as well as drug transport at the boundaries of the unit. In section 3, we study the effect of several factors on drug distribution within the brain ECF. In section 3.1, we evaluate the effect of the brain capillary blood flow velocity on local brain ECF PK in the 3D brain unit. Next, we evaluate the effect of active influx and efflux on local brain ECF PK (section 3.2). Then, in section 3.3 we show how the interplay between the brain capillary blood flow velocity, passive BBB permeability and active transport affects drug concentrations within the 3D brain unit. Finally, in section 4 we conclude our work and discuss future perspectives.

2 The 3D brain unit

The 3D brain unit represents the smallest piece of brain tissue that contains all physiological elements of the brain. The 3D brain unit is part of a larger network of 3D brain units, but here we focus on just one 3D brain unit that is fed by an arteriole and drained by a venule (Fig 1, left). The 3D brain unit is a cube in which the brain capillaries (represented by red rectangular boxes on the ribs) surround the brain ECF (Fig 1, left). The segments of red rectangular boxes protruding from the vertices from the 3D brain unit are parts of brain capillaries from neighbouring units. As such, each vertex connects three incoming brain capillaries to three outgoing brain capillaries, with the exception of the vertex connected to the arteriole and the vertex connected to the venule. These connect the arteriole to three outgoing brain capillaries and three incoming brain capillaries to the venule, respectively.

A single 3D brain unit (Fig 1, middle) has a blood-plasma-domain (red) consisting of multiple sub-domains. These include the brain capillary domain where drug enters the unit (indicated by U_{in} in Fig 1), the domains representing the x-directed, y-directed and z-directed brain capillaries (indicated by $U_{\text{x1–x4}}$, $U_{\text{y1–y4}}$ and $U_{\text{z1–z4}}$ in Fig 1) and the brain capillary domain where drug leaves the unit (indicated by U_{out} in Fig 1). Drug within the blood plasma

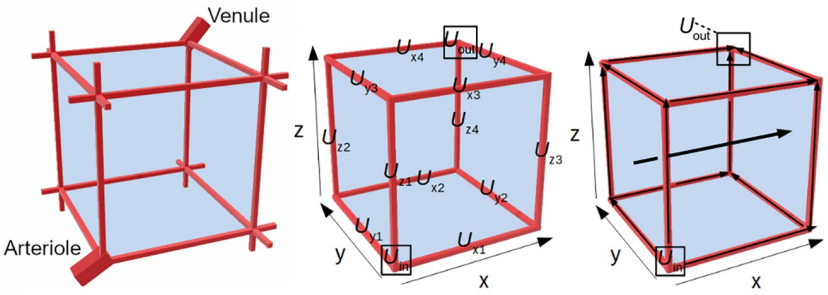

Fig 1. Sketch of the 3D model brain unit. Left: The structure represented by the 3D brain unit. An arteriole carries blood plasma (containing drug) into a brain capillary bed, that is connected to a venule that drains the blood plasma. The brain capillaries (red) surround the brain ECF (blue). Middle: the 3D brain unit and its sub-domains. The unit consists of a brain-ECF-domain (blue) and a blood-plasma-domain (red). The blood-plasma-domain is divided into several subdomains: U_{in} is the domain where the dose of absorbed drug enters the 3D brain unit, $U_{x1\text{-}x4}$, $U_{y1\text{-}y4}$ and $U_{z1\text{-}z4}$ are the domains representing the x-directed, y-directed and z-directed capillaries, respectively. Right: Directions of transport in the model. The drug enters the brain capillaries in U_{in}. From there, it is transported through the brain capillaries by the brain capillary blood flow in the direction indicated by the small arrows. Drug in the brain capillary blood plasma exchanges with the brain ECF by crossing the BBB. Drug within the brain ECF is, next to diffusion, transported along with brain ECF bulk flow (indicated by the bold arrow).

https://doi.org/10.1371/journal.pone.0238397.g001

is transported by the brain capillary blood flow. The brain capillary blood flow splits at the vertices of the unit, where brain capillary branching occurs (Fig 1, right).

In developing the model, we make the following assumptions about drug distribution within the brain capillaries:

Assumptions 1.

(i) *The drug concentration within the blood plasma changes as a function of time depending on dose, bioavailability, the rate of absorption (in case of oral administration), distribution volume and elimination into and from the blood plasma.*

(ii) *The blood carrying the drug flows into 3D brain unit by a feeding arteriole and leaves via a draining venule (* Fig 1, *left).*

(iii) *The drugs enters the brain unit in the domain U_{in} (* Fig 1, *middle), and drug concentrations in U_{in} are unaffected by the brain capillary blood flow.*

(iv) *The brain capillary blood flow is directed away from U_{in} (* Fig 1, *right).*

(v) *In the blood plasma, drug transport by diffusion is negligible compared to drug transport by the brain capillary blood flow.*

(vi) *The brain capillary blood flow velocity is by default equal in all brain capillaries.*

(vii) *Drug within the blood plasma does not bind to blood plasma proteins. All drug within the blood plasma is in an unbound state and is able to cross the BBB.*

Drug within the blood plasma of the brain capillaries crosses the BBB to exchange with the brain ECF. The BBB is located at the border between the brain capillaries (red) and the brain ECF (blue), see Fig 1. Drug exchange between the blood plasma and the brain ECF is described by passive and active transport across the BBB in both directions. Here, we assume that active influx transporters move a compound from the blood plasma directly into the brain ECF and that active efflux transporters move a compound from the brain ECF directly into the blood plasma.

Within the brain ECF, we formulate:

Assumptions 2.

(i) *Drug within the brain ECF is transported by diffusion and brain ECF bulk flow.*

(ii) *Cells are not explicitly considered, but only by taking the tortuosity (hindrance on diffusion imposed by the cells) into account.*

(iii) *The brain ECF bulk flow is unidirectional. It is pointed in the x-direction, see the bold arrow in Fig 1 (right).*

(iv) *All drug distributes within the brain ECF and we only have extracellular binding sites.*

(v) *The total concentration of specific and non-specific binding sites is constant.*

(vi) *The specific and non-specific binding sites are evenly distributed over the 3D brain unit and do not change position.*

(vii) *The specific and non-specific binding sites lie on the outside of cells and the drug does not have to cross cell membranes in order to bind to binding sites.*

(viii) *Drug binding is reversible and drugs associate and dissociate from their binding sites.*

2.1 Formulation of the 3D brain unit

The 3D brain unit is a cubic domain, U, that represents a piece of brain tissue. We define $U = \{(x,y,z) \in \mathbb{R}^3 \mid 0 \leq x \leq x_r \wedge 0 \leq y \leq y_r \wedge 0 \leq z \leq z_r\}$. There, x_r, y_r and z_r are constants that represent the length of one unit and are defined as $d_{cap}+2r$, with d_{cap} the distance between the brain capillaries and r the brain capillary radius. In one brain unit, the brain capillaries, the BBB and the brain ECF are represented by the subsets $U_{pl} \subset U$, $U_{BBB} \subset U$ and $U_{ECF} \subset U$, respectively, such that $U = U_{pl} \cup U_{BBB} \cup U_{ECF}$.

Within U_{pl}, we define U_{in} as the domain where the blood plasma, containing drug, enters the 3D brain unit from a feeding arteriole. We define U_{out} as the domain where the blood plasma, containing drug, leaves the 3D brain unit to a draining venule. Additionally, we define the x-directed, y-directed and z-capillaries as the sets $\{U_{xi}, i = 1,..,4\}$, $\{U_{yi}, i = 1,..,4\}$ and $\{U_{zi}, i = 1,..,4\}$. The brain capillaries are divided by the lines $x = y$ (or $y = z$ or $x = z$) and $x+y = y_r$ (or $y+z = z_r$ or $x+z = z_r$), for which an example is shown in Fig 2. The only exceptions for this are the brain capillaries adjacent to U_{in} and U_{out}, see below.

The definitions of the regions are as follows:

$U_{x1} = \{(x,y,z) \in U \mid r \leq x < x_r-y, r \leq x < x_r-z \wedge 0 \leq y < r \wedge 0 \leq z < r\}$

$U_{x2} = \{(x,y,z) \in U \mid y_r-y < x \leq y \wedge z \leq x < x_r-z \wedge y_r \geq y > y_r-r \wedge 0 \leq z < r\}$

$U_{x3} = \{(x,y,z) \in U \mid y \leq x < x_r-y \wedge z_r-z < x \leq z \wedge 0 \leq y < r \wedge z_r \geq z > z_r-r\}$

$U_{x4} = \{(x,y,z) \in U \mid y_r-y < x \leq y \wedge z_r-z < x \leq z \wedge y_r \geq y > y_r-r \wedge z_r \geq z > z_r-r\}$

$U_{y1} = \{(x,y,z) \in U \mid r \leq y < y_r-z \wedge r \leq y \leq y_r x \wedge 0 \leq x < r \wedge 0 \leq z < r\}$

$U_{y2} = \{(x,y,z) \in U \mid z \leq y < y_r-z \wedge x_r-x \leq y < x \wedge x_r \geq x > x_r-r \wedge 0 \leq z < r\}$

$U_{y3} = \{(x,y,z) \in U \mid z_r-z < y \leq z \wedge x < y \leq y_r-x \wedge 0 \leq x < r \wedge z_r \geq z > z_r-r\}$

$U_{y4} = \{(x,y,z) \in U \mid z_r-z \leq y < z \wedge x_r-x < y \leq x \wedge x_r \geq x > x_r-r \wedge z_r \geq z > z_r-r\}$

$U_{z1} = \{(x,y,z) \in U \mid r \leq z \leq z_r-x \wedge r \leq z \leq z_r-y \wedge 0 \leq x < r \wedge 0 \leq y < r\}$

$U_{z2} = \{(x,y,z) \in U \mid x < z \leq z_r-x \wedge y_r-y \leq z < y \wedge 0 \leq x < r \wedge y_r \geq y > y_r-r\}$

$U_{z3} = \{(x,y,z) \in U \mid x_r-x \leq z < x \wedge y < z \leq z_r-y \wedge x_r \geq x > x_r-r \wedge 0 \leq y < r\}$

$U_{z4} = \{(x,y,z) \in U \mid x_r-x \leq z < x \wedge y_r-y \leq z < y \wedge x_r \geq x > x_r-r \wedge y_r \geq y > y_r-r\}$

$U_{in} = \{(x,y,z) \in U \mid 0 \leq x < r \wedge 0 \leq y < r \wedge 0 \leq z < r\}$

$U_{out} = \{(x,y,z) \in U \mid x_r-r \leq x < x_r \wedge y_r-r \leq y < y_r \wedge z_r-r \leq z < z_r\}$.

The BBB is represented by a subset $U_{BBB} \subset U$, such that $U_{BBB} = \partial U_{pl} \backslash \partial U$. This denotes the border between the blood plasma and the brain ECF, located at distance r from the edges of the 3D brain unit.

The brain ECF is represented by a subset $U_{ECF} \subset U$, such that $U_{ECF} = U \backslash (U_{pl} \cup U_{BBB})$.

Within U we define the following quantities describing drug concentration:

C_{pl} (x,y,z,t): $U_{pl} \times \mathbb{R}^+ \rightarrow \mathbb{R}^+$,

C_{ECF} (x,y,z,t): $U_{ECF} \times \mathbb{R}^+ \rightarrow \mathbb{R}^+$,

B_1 (x,y,z,t): $U_{ECF} \times \mathbb{R}^+ \rightarrow \mathbb{R}^+$,

B_2 (x,y,z,t): $U_{ECF} \times \mathbb{R}^+ \rightarrow \mathbb{R}^+$.

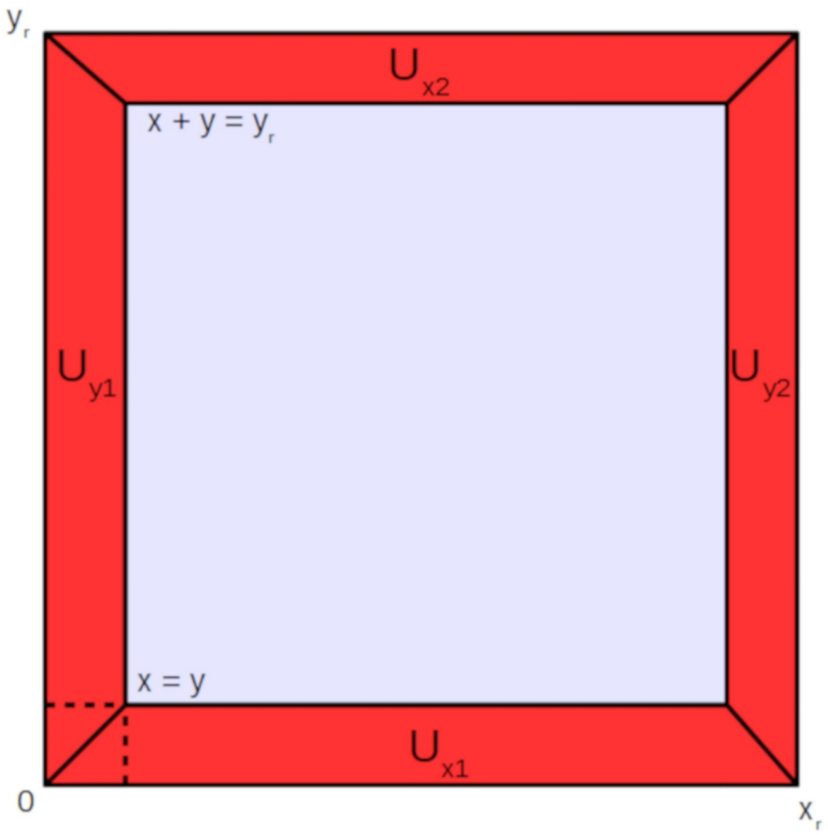

Fig 2. Front view of the 3D brain unit. Definitions of U_{pl} are given. The x-directed, y-directed and z-capillaries are divided by the lines x = y (or y = z or x = z) and x+y = y_r (or y+z = z_r or x+z = z_r). The only exceptions for this are the brain capillaries adjacent to U_{in} and the brain capillaries adjacent to U_{out}.

https://doi.org/10.1371/journal.pone.0238397.g002

Here, C_{pl} is the concentration of unbound drug in the blood plasma, C_{ECF} is the concentration of unbound drug in the brain ECF, B_1 is the concentration of drug in the brain ECF bound to specific binding sites and B_2 is the concentration of drug in the brain ECF bound to non-specific binding sites.

2.2 Description of drug distribution in U_{pl}

Based on assumptions 1(i) and 1(iii), we describe the concentration of unbound drug within U_{in} by including parameters related to single oral administration [32] using the Bateman function [33]:

$$C_{pl} = \frac{Fk_a Dose}{V_d(k_a - k_e)}\left(e^{-k_e t} - e^{-k_a t}\right) \text{ for } C_{pl} \in U_{in}, \quad (1)$$

where F is the bioavailability of the drug, k_a the absorption rate constant of the drug, k_e the elimination rate constant of the drug, *Dose* the molar amount of orally administered drug, and V_d the distribution volume, which relates the total amount of drug in the body to the drug concentration in the blood plasma. We focus on single oral administration but can also study other choices.

Additionally, based on assumptions 1(iv) and 1(v), we define:

$$\frac{\mathrm{d}C_{\mathrm{pl}}}{\mathrm{dt}} = -v_{\mathrm{blood}}\frac{\partial C_{\mathrm{pl}}}{\partial \mathrm{x}} \text{ for } C_{\mathrm{pl}} \in U_{\mathrm{xi}}, \text{ for } \mathrm{i} = 1, 4, \tag{2}$$

$$\frac{\mathrm{d}C_{\mathrm{pl}}}{\mathrm{dt}} = -v_{\mathrm{blood}}\frac{\partial C_{\mathrm{pl}}}{\partial \mathrm{y}} \text{ for } C_{\mathrm{pl}} \in U_{\mathrm{yi}}, \text{ for } \mathrm{i} = 1, 4, \tag{3}$$

$$\frac{\mathrm{d}C_{\mathrm{pl}}}{\mathrm{dt}} = -v_{\mathrm{blood}}\frac{\partial C_{\mathrm{pl}}}{\partial \mathrm{z}} \text{ for } C_{\mathrm{pl}} \in U_{\mathrm{zi}}, \text{ for } \mathrm{i} = 1, 4, \tag{4}$$

with v_{blood} the blood flow velocity within the brain capillaries and where the initial condition is given by

$$C_{\mathrm{pl}}(\mathrm{x}, \mathrm{y}, \mathrm{z}, \mathrm{t} = 0) = 0. \tag{5}$$

2.3 Description of drug distribution in U_{ECF}

Based on assumptions 2, we describe the distribution of unbound and bound drug within U_{ECF} with the following system of equations:

$$\begin{aligned} \frac{\partial C_{\mathrm{ECF}}}{\partial t} &= \frac{D}{\lambda^2}\nabla^2 C_{\mathrm{ECF}} - v_{\mathrm{ECF}}\frac{\partial C_{\mathrm{ECF}}}{\partial \mathrm{x}} - k_{1\mathrm{on}}C_{\mathrm{ECF}}(B_1^{\max} - B_1) + k_{1\mathrm{off}}B_1 \\ &\quad -k_{2\mathrm{on}}C_{ECF}(B_2^{\max} - B_2) + k_{2\mathrm{off}}B_2 \\ \frac{\partial B_1}{\partial t} &= k_{1\mathrm{on}}C_{\mathrm{ECF}}(B_1^{\max} - B_1) - k_{1\mathrm{off}}B_1 \\ \frac{\partial B_2}{\partial t} &= k_{2\mathrm{on}}C_{\mathrm{ECF}}(B_2^{\max} - B_2) - k_{2\mathrm{off}}B_2. \end{aligned} \tag{6}$$

with initial conditions

$$C_{\mathrm{ECF}}(\mathrm{x}, \mathrm{y}, \mathrm{z}, \mathrm{t} = 0) = 0, \tag{7}$$

$$B_{\mathrm{i}}(\mathrm{x}, \mathrm{y}, \mathrm{z}, \mathrm{t} = 0) = 0, \mathrm{i} = 1, 2, \tag{8}$$

where D is the diffusion coefficient in a free medium, λ the tortuosity, v_{ECF} the (x-directed) brain ECF bulk flow, ${B_1}^{\max}$, the total concentration of specific binding sites within the brain ECF, $k_{1\mathrm{on}}$ the association rate constant for specific binding, $k_{1\mathrm{off}}$ the dissociation rate constant for specific binding, ${B_2}^{\max}$ the total concentration of non-specific binding sites within the brain ECF, $k_{2\mathrm{on}}$ the association rate constant for non-specific binding and $k_{2\mathrm{off}}$ the dissociation rate constant for non-specific binding.

2.4 Boundary conditions

We formulate boundary conditions that describe the change in concentration of drug at the boundary between the blood-plasma-domain (U_{ok}) and the brain-ECF-domain (U_{ECF}), hence at U_{BB} as well as at the boundaries of the 3D brain unit ($U_{\mathrm{pl}} \cap \partial\, U$, $U_{\mathrm{ECF}} \cap \partial U$).

2.4.1 Drug exchange between U_{pl} and U_{ECF}. We describe diffusive transport by the difference in drug concentrations in C_{ECF} and C_{pl}, multiplied by the BBB permeability, P. In

addition, we model active transport into and out of the brain ECF with Michaelis-Menten kinetics, as they are well established and match with most available data on parameters related to BBB active transport, similar to the approach of [6]. In total, this leads to:

$$\begin{aligned} \mathrm{f}(\mathrm{u},\mathrm{v}) &= P(\mathrm{u}-\mathrm{v}) + \frac{T_{\mathrm{m-in}}}{SA_{\mathrm{BBB}}(K_{\mathrm{m-in}}+\mathrm{u})}\mathrm{u} - \frac{T_{\mathrm{m-out}}}{SA_{\mathrm{BBB}}(K_{\mathrm{m-out}}+\mathrm{v})}\mathrm{v}, \\ \text{with} \quad P &= P_{\mathrm{trans}}f_{\mathrm{trans}} + P_{\mathrm{para}}f_{\mathrm{para}}, \\ \text{with} \quad P_{\mathrm{para}} &= \frac{D_{\mathrm{para}}}{W_{\mathrm{PCS}}}, \end{aligned} \tag{9}$$

with u = C_{pl}, v = C_{ECF}, P_{trans} being the permeability through the brain endothelial cells, f_{trans} the fraction of the area occupied by the brain endothelial cells, D_{para} the diffusivity of a drug across the paracellular space, W_{PCS} the width of the paracellular space, f_{para} the fraction of area occupied by the paracellular space, $T_{\mathrm{m\text{-}in}}$ the maximum rate of drug active influx, $T_{\mathrm{m\text{-}out}}$ the maximum rate of drug active efflux, $K_{\mathrm{m\text{-}in}}$ the concentration of drug at which half of $T_{\mathrm{m\text{-}in}}$ is reached, $K_{\mathrm{m\text{-}out}}$ the concentration of drug at which half of $T_{\mathrm{m\text{-}out}}$ is reached and SA_{BBB} the surface area of the BBB.

Based hereon, we describe the loss or gain of unbound drug in the brain ECF due to BBB transport with the following boundary conditions (only those for the x direction are given, the ones for the y and z directions are similar):

$$\begin{aligned} -D^{*}\frac{\partial C_{\mathrm{ECF}}}{\partial \mathrm{x}} &= \mathrm{f}(\mathrm{C_{pl}},\mathrm{C_{ECF}}) \quad \text{for } (\mathrm{x},\mathrm{y},\mathrm{z}) \in U_{\mathrm{BBB}} \text{ at } \mathrm{x}=\mathrm{r}, \\ D^{*}\frac{\partial C_{\mathrm{ECF}}}{\partial \mathrm{x}} &= \mathrm{f}(\mathrm{C_{pl}},\mathrm{C_{ECF}}) \quad \text{for } (\mathrm{x},\mathrm{y},\mathrm{z}) \in U_{\mathrm{BBB}} \text{ at } \mathrm{x}=x_{\mathrm{r}}-\mathrm{r}. \end{aligned} \tag{10}$$

For the blood-plasma-domain, U_{pl}, we use the reverse of (10) to describe drug transport across the BBB in the brain capillaries with the following boundary conditions:

$$\begin{aligned} D^{*}\frac{\partial C_{\mathrm{pl}}}{\partial \mathrm{x}} &= \mathrm{f}(\mathrm{C_{pl}},\mathrm{C_{ECF}}) \quad \text{for } (\mathrm{x},\mathrm{y},\mathrm{z}) \in U_{\mathrm{BBB}} \text{ at } \mathrm{x}=\mathrm{r}, \\ D^{*}\frac{\partial C_{\mathrm{pl}}}{\partial \mathrm{x}} &= -\mathrm{f}(\mathrm{C_{pl}},\mathrm{C_{ECF}}) \quad \text{for } (\mathrm{x},\mathrm{y},\mathrm{z}) \in U_{\mathrm{BBB}} \text{ at } \mathrm{x}=x_{\mathrm{r}}-\mathrm{r}. \end{aligned} \tag{11}$$

2.4.2 Drug exchange at the faces of the 3D brain unit. We use additional boundary conditions to describe the drug concentrations at the sides of the domain. Since we assume that there is no diffusion in the blood plasma (see assumption 1(v)), we use the following boundary conditions:

$$\frac{\partial C_{\mathrm{pl}}}{\partial \mathrm{x}} = 0, \tag{12}$$

for (x,y,z) $\in U_{\mathrm{pl}} \backslash U_{\mathrm{out}} \cap \partial U$ at x = 0 and x = $\mathrm{x_r}$,

$$\frac{\partial C_{\mathrm{pl}}}{\partial \mathrm{y}} = 0, \tag{13}$$

for (x,y,z) $\in U_{pl} \setminus U_{out} \cap \partial U$ at y = 0 and y = y_r,

$$\frac{\partial C_{pl}}{\partial z} = 0, \tag{14}$$

for (x,y,z) $\in U_{pl} \setminus U_{out} \cap \partial U$ at z = 0 and z = z_r.

In addition, we define:

$$C_{pl} = 0, \tag{15}$$

for (x,y,z) $\in U_{out} \cap \partial U$.

We formulate the condition at the boundaries of the 3D brain unit as follows:

$$\mathbf{n} \cdot \nabla C_{ECF} = 0 \text{ for } (x, y, z) \in U_{ECF} \cap \partial U \tag{16}$$

and where n is the normal vector on $U_{ECF} \cap \partial U$.

2.5 Model parameter values and units

The dimensions of the 3D brain unit are based on the properties of the rat brain. The model is suitable for data from human or other species as well, but we have chosen for the rat as for this species most data is available. The distance between the brain capillaries in the rat brain is on average 50 μm, while the brain capillaries have a radius of about 2.5 μm [34–37]. Therefore, we set the radius of the brain capillaries, r, to 2.5 μm and the dimensions of the 3D brain unit in the x, y and z directions, x_r, y_r and z_r respectively, to 55 μm.

In our model, we use Eqs (1)–(5) to describe drug concentration within the blood plasma, with boundary conditions described in Eqs (11)–(15). We describe the concentration of drug within the brain ECF with Eqs (6)–(8) with boundary conditions described in (9), (10) and (16). The range of values we use for the parameters in the model as well as their units are given in Table 1 below. This range is based on values found in the literature (from experimental studies), which we also give in the table. The literature does not provide values on the kinetic parameters related to non-specific binding kinetics (B_2^{max}, k_{2on} and k_{2off}). Therefore, we base the choices of these values on earlier articles that assume that drug binding to specific binding sites is stronger than to non-specific binding sites, while non-specific binding sites are more abundant [31, 38, 39].

3 Model results

We study the distribution of a drug within the 3D brain unit by plotting its concentration-time profiles within the brain ECF (brain ECF PK). In addition, we study the distribution of the drug within the 3D brain unit. We first nondimensionalise the system of equations and boundary conditions by scaling all variables by a characteristic scale, see S1 Appendix for details. Next, in order to perform simulations, we discretise the nondimensionalised system spatially, using a well-established numerical procedure based on finite element approximations [66]. After weighing accuracy and computational cost, as well as taking into account that small changes in resolution of the computational mesh should not substantially affect the simulation results, we chose a resolution of 18 lines per dimension to proceed with in the simulations. We present the results using the parameters with dimensions. The output of the simulations are the concentrations of free, specifically bound and non-specifically bound drug, given in μmol L^{-1} over time (s).

The model can easily be used to study a specific drug by choosing the parameter values that are specific for this drug, provided that parameter values for this drug are known. In the present study, however, we choose to study generic parameter values that are in the middle of the

Table 1. 3D brain unit model parameters and their units, for rat brain. The physiological range of values of the parameters is given. These are based on references from the literature. All parameters depend on both drug-specific and system-specific properties, except for d_{cap},r, v_{blood}, v_{ECF}, $T_{m\text{-}in}$, $T_{m\text{-}out}$, SA_{BBB},B_1^{max} and B_2^{max}, which depend on system-specific properties only.

Parameter	Unit	Range of values	Ref.
F, bioavailability	-	0-1	[32]
Dose	μmol	10^{-1}-10^{2}	
V_d, distribution volume	L	0.05-5	[40]
k_a, absorption rate constant	s^{-1}	0-$2{\cdot}10^{-3}$	[40]
			[20]
k_e, elimination rate constant	s^{-1}	$5{\cdot}10^{-5}$-$3{\cdot}10^{-2}$	[40]
			[20]
d_{cap}, intercapillary distance	m	$2{\cdot}10^{-5}$-$7{\cdot}10^{-5}$	[34]
			[41]
r, brain capillary radius	m	0.8-$4.8{\cdot}10^{-6}$	[41]
			[37]
v_{blood}, brain capillary blood flow velocity	m s^{-1}	0.5-$50{\cdot}10^{-4}$	e.g. [5]
$D^* = \frac{D}{\lambda^2}$, effective diffusion coefficient	m^2s^{-1}	10^{-11}-10^{-10}	[42]
			[43]
v_{ECF}, brain ECF bulk flow velocity	m s^{-1}	$5{\cdot}10^{-8}$-$5{\cdot}10^{-6}$	[44]
			[45]
P, 3D passive BBB permeability[1]	m s^{-1}	10^{-10}-10^{-5}	[46][2]
$T_{m\text{-}in}$, maximal active influx rate	μmol s^{-1}	10^{-8}-10^{-5}	[47]
$K_{m\text{-}in}$, concentration needed to reach half of $T_{m\text{-}in}$	μmol L^{-1}	10^{1}-10^{4}	[48]
$T_{m\text{-}out}$, maximal active efflux rate	μmol s^{-1}	10^{-8}-10^{-5}	[47]
$K_{m\text{-}out}$, concentration needed to reach half of $T_{m\text{-}out}$	μmol L^{-1}	10^{1}-10^{4}	[48]
SA_{BBB} surface area of the BBB[6]	m^2	$1.25{\cdot}10^{-10}$	
B_1^{max}, total concentration specific binding sites	μmol L^{-1}	$1{\cdot}10^{-3}$-$5{\cdot}10^{-1}$	[16][3]
k_{1on}, specific association constant	(μmol $L^{-1}s)^{-1}$	10^{-4}-10^{2}	[16][4]
k_{1off}, specific dissociation constant	s^{-1}	10^{-6}-10^{1}	[16][4]
B_2^{max}, total concentration non-specific binding sites	μmol L^{-1}	$1{\cdot}10^{1}$-$5{\cdot}10^{3}$	[31]
k_{2on}, non-specific association constant	(μmol $L^{-1}s)^{-1}$	10^{-6}-10^{1}	[31]
k_{2off}, non-specific dissociation constant	s^{-1}	10^{-4}-10^{3}	[31]

[1]This value is the apparent (experimentally measured) overall passive permeability [46].

[2] [49–52]

[3] [53–58]

[4] http://www.k4dd.eu and [59]

[5] [60–64], [65]

[6]This is the surface area of the BBB that separates one side of a brain capillary within the 3D brain unit from the brain ECF.

https://doi.org/10.1371/journal.pone.0238397.t001

physiological ranges given in Table 1. This allows us to perform a sensitivity analysis and study the effect of parameter values at both extremes of the physiological range on the behaviour of the model. We use, unless otherwise indicated, the parameter values that are given in Table 2.

In the following sections, we show the impact of the brain capillary blood flow velocity (v_{blood}) in the absence of active transport (section 3.1), the impact of active transport (section 3.2) and the impact of v_{blood} and active transport combined (section 3.3) on blood plasma and brain ECF PK and brain ECF drug distribution. We give the concentration-time profiles of unbound drug, specifically bound drug and non-specifically bound drug in the middle of

U_{ECF}, where $(x, y, z) = \left(\frac{x_t}{2}, \frac{y_t}{2}, \frac{z_t}{2}\right)$ as well as those of unbound drug in the blood plasma in the middle of U_{x1}, where $(x, y, z) = \left(\frac{x_t}{2}, \frac{r}{2}, \frac{r}{2}\right)$, on a log-scale versus time. Drug distribution profiles are given for cross-sections of the entire (x,y,z)-domain of the 3D brain unit for various times.

3.1 The effect of the brain capillary blood flow velocity on brain ECF PK within the 3D brain unit

The impact of the brain capillary blood flow velocity, v_{blood}, on brain ECF PK within the 3D brain unit is evaluated. Parameters are as in Table 2 and we thus assume that there is no active transport, i.e. $T_{m\text{-}in} = 0$ and $T_{m\text{-}out} = 0$. Here, we focus on the effect of v_{blood} on brain ECF PK in the middle of the 3D brain unit. We show the concentration-time profiles of unbound, specifically bound and non-specifically bound drug (C_{ECF}, B_1 and B_2, respectively) within the 3D brain unit on a larger time-scale, for several values of v_{blood}. We do so for the default value of the passive permeability P ($P = 0.1{\cdot}10^{-7}$ m s^{-1}), in Fig 3 (left), as well as for a high value of P ($P = 100{\cdot}10^{-7}$ m s^{-1}), in Fig 3 (right). The lowest value of v_{blood} is outside the known physiological ranges (see Table 1), but we choose it as v_{blood} is predicted to mostly impact drug concentrations in the brain when P is much higher than v_{blood} [67, 68]. The total passive permeability, P, includes both transcellular and paracellular permeability. The paracellular space may increase due to disruption of the tight junctions in certain disease conditions, thereby allowing larger molecules to pass through and increasing paracellular transport [69, 70]. We can tune

Table 2. 3D brain unit model default parameter values and their units. The values are for a hypothetical drug and are all within the physiological ranges given in Table 1.

Parameter	Unit	Value
F	-	1
$Dose$	μmol	0.5
k_a	s^{-1}	$2{\cdot}10^{-4}$
k_e	s^{-1}	$5{\cdot}10^{-5}$
V_d	L	0.2
d_{cap}	m	$5{\cdot}10^{-5}$
r	m	$2.5{\cdot}10^{-6}$
v_{blood}	m s^{-1}	$5{\cdot}10^{-4}$
D^*	m^{2}s^{-1}	$0.5{\cdot}10^{-10}$
v_{ECF}	m s^{-1}	$0.5{\cdot}10^{-6}$
P	m s^{-1}	$0.1{\cdot}10^{-7}$
f_{para}		0.006
f_{trans}		0.994
$T_{m\text{-}in}$	μmol s^{-1}	$0{\cdot}10^{-7}$
$T_{m\text{-}out}$	μmol s^{-1}	$0{\cdot}10^{-7}$
$K_{m\text{-}in}$	μmol L^{-1}	$1{\cdot}10^{2}$
$K_{m\text{-}out}$	μmol L^{-1}	$1{\cdot}10^{2}$
SA_{BBB}	m^2	$1{\cdot}10^{-10}$
B_1^{max}	μmol L^{-1}	$5{\cdot}10^{-2}$
k_{1on}	(μmol L^{-1}s)$^{-1}$	1
k_{1off}	s^{-1}	$1{\cdot}1^{-2}$
B_2^{max}	μmol L^{-1}	$5{\cdot}10^{1}$
k_{2on}	(μmol L^{-1}s)$^{-1}$	$1{\cdot}10^{-2}$
k_{2off}	s^{-1}	1

https://doi.org/10.1371/journal.pone.0238397.t002

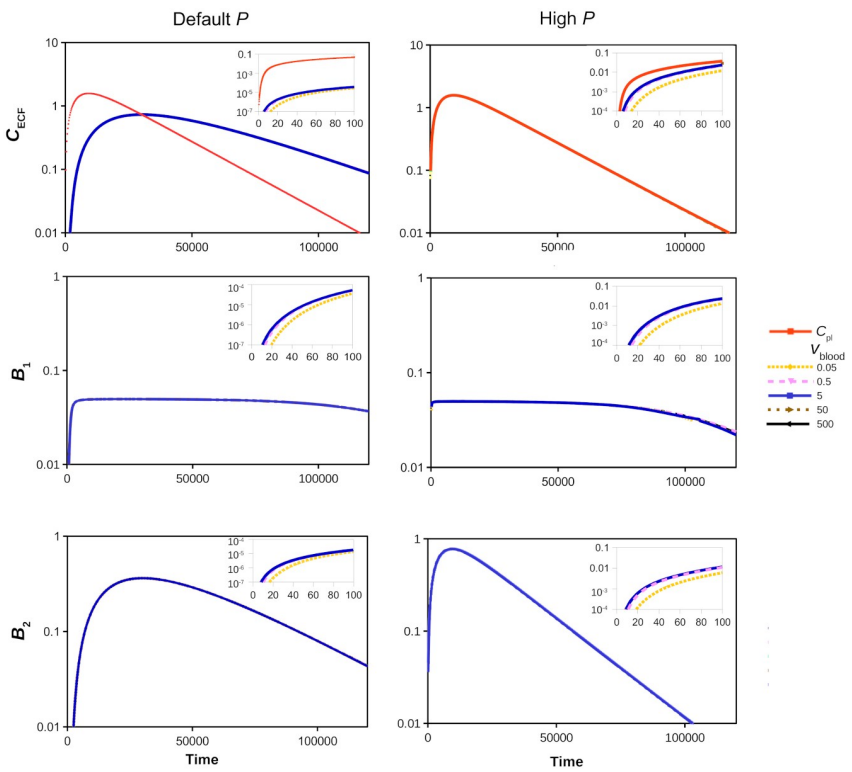

Fig 3. The effect of the brain capillary blood flow velocity, v_{blood} (m s^{-1}), on the log PK of C_{pl} (red) and C_{ECF} (top), B_1 (middle) and B_2 (bottom) for a default ($P = 0.1 \cdot 10^{-7}$ m s^{-1}) (left) and a high ($P = 100 \cdot 10^{-7}$ m s^{-1}) (right) value of P. Values of v_{blood} are set at $0.05 \cdot 10^{-4}$ m s^{-1}, $0.5 \cdot 10^{-4}$ m s^{-1}, $5 \cdot 10^{-4}$ m s^{-1}, $50 \cdot 10^{-4}$ m s^{-1} and $500 \cdot 10^{-4}$ m s^{-1}, as is depicted by different colours, where drug concentrations for the default value of v_{blood} ($v_{blood} = 5 \cdot 10^{-4}$ m s^{-1}) are shown in blue. All other parameters are as in Table 2. The insets in each sub-figure show the PK for a shorter time.

https://doi.org/10.1371/journal.pone.0238397.g003

our model and separate between transcellular and paracellular transport, as we do in S2 Appendix. In the current section we proceed with the total passive BBB permeability.

Fig 3 shows that v_{blood} does not impact long-time behaviour of C_{ECF}, B_1 and B_2. The insets in Fig 3 demonstrate that v_{blood} impacts short-time (t = 0-100 s) behaviour only when it has extremely low values ($v_{blood} \leq 0.5 \cdot 10^{-4}$ m s^{-1}), as depicted in the insets of Fig 3 by the yellow and purple lines, respectively. The impact of v_{blood} on C_{ECF}, B_1 and B_2 is independent of the values of P (compare the left and right insets of Fig 3). The effects of P on drug concentrations within the brain ECF are similar to those found with our proof-of-concept 2D model [31]: for a high value of P, the attained values of C_{ECF} and B_2 are higher and follow C_{pl}, while their decay is faster than for a low value of P. In addition, the $\geq$90% maximum value of B_1, i.e. values of B_1 that are more than 90% of the maximum value attained during the simulation ($B_1 \geq 90\%$ max (B_1)), is attained shorter for a high value of P than for a low value of P.

From the results shown in Fig 3 we conclude that the effects of v_{blood} on brain ECF PK are minimal. According to the Renkin-Crone equation [67, 68], the brain capillary blood flow affects drug *influx*, depending on the permeability of the BBB. This is also demonstrated by our model, and we show that v_{blood} affects drug influx across the BBB in S3 Appendix.

The plots in Fig 4a show the changes in concentration of drug within the blood plasma over a short time-range (t = 5 to t = 25). There, C_{pl} is plotted along the capillaries starting at U_{in} (where drug enters the unit) to U_{out} (where drug exits the unit). We measure the distance from U_{in}, where the total distance between these points is 150 μm. Drug can be transported along

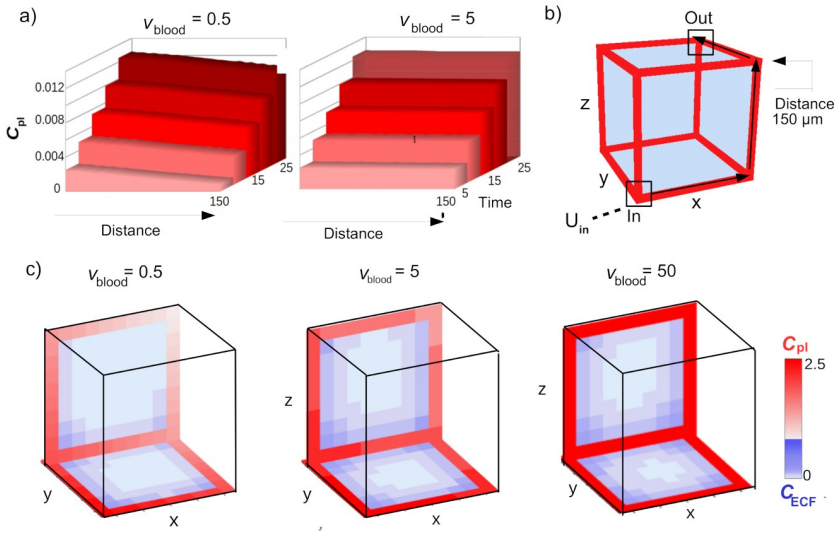

Fig 4. Changes in C_{pl} and C_{ECF} due to the effect of v_{blood}. While v_{blood} is varied from $0.05{\cdot}10^{-4}$ m s^{-1} to $50{\cdot}10^{-4}$ m s^{-1}, all other parameter values are as in Table 2. a) The pathway from U_{in} to U_{out} along which C_{pl} is plotted. b) C_{pl} is plotted against time (timepoints from 5 to 25) along the distance shown in (a). c) Distribution profiles of C_{pl} (red) and C_{ECF} (blue) of the 3D brain unit at t = 5. Darker shades of red and blue correspond to higher values of C_{pl} and C_{ECF}, respectively.

https://doi.org/10.1371/journal.pone.0238397.g004

several pathways, but in Fig 4a the values of C_{pl} are given along the pathway indicated in Fig 4b. When v_{blood} = 0.5 (left), there are clear differences between C_{pl} in U_{in} (Distance = 0) and C_{pl} in the opposite corner (Distance = 150) at the time-points shown. However, as C_{pl} increases over time, the differences in C_{pl} become small relative to the value of C_{pl}. Fig 4c shows the distribution profiles of unbound drug within the 3D brain unit at t = 5 for different values of v_{blood}. There, darker shades of red and blue correspond to higher concentrations of unbound drug in the blood plasma and the brain ECF, respectively. When $v_{blood} = 0.5{\cdot}10^{-4}$ m s^{-1}, the transport time of drug between U_{in} and the opposite corner is higher than when $v_{blood} = 5{\cdot}10^{-4}$ m s^{-1}. This is depicted in Fig 4c, where at t = 5, drug concentrations within U_{pl} are equal for a high brain capillary blood flow velocity ($v_{blood} = 50{\cdot}10^{-4}$ m s^{-1}), while local differences in C_{pl} still exist for a low value of v_{blood} ($v_{blood} = 0.5{\cdot}10^{-4}$ m s^{-1}). The value of v_{blood} also affects local concentrations of C_{ECF}. For a low value of v_{blood} ($v_{blood} = 0.5{\cdot}10^{-4}$ m s^{-1}), values of C_{ECF} at t = 5 are overall low, but highest in the corners closest to U_{in}. For higher values of v_{blood} ($v_{blood} = 5{\cdot}10^{-4}$ m s^{-1} and $v_{blood} = 50{\cdot}10^{-4}$ m s^{-1}), C_{ECF} at t = 5 is overall higher, but again highest in the corner close to U_{in}.

3.2 The effect of active transport on the drug concentrations within the brain ECF

Active transport kinetics are regulated by the maximal transport rate (T_m) and the concentration of drug needed to reach half of the maximal transport rate (K_m), see section 2.4.1. We first focus on active influx, such that $T_{m\text{-}out} = 0$. We vary $T_{m\text{-}in}$, which denotes the maximal rate of active transporters moving drug from the blood plasma *into* the brain ECF. Fig 5 shows the effects of increasing values of $T_{m\text{-}in}$ (starting at $T_{m\text{-}in} = 0$, i.e. no active influx) on C_{ECF} (top), B_1 (middle) and B_2 (bottom). Fig 5 (top) reveals that an increased value of $T_{m\text{-}in}$ correlates with increased concentrations of C_{ECF}. The time to the peak of C_{ECF} is not affected by the value of $T_{m\text{-}in}$. Fig 5 (middle) shows that $T_{m\text{-}in}$ does affect the time during which the specific binding sites are saturated. We find that 90% max(B_1) is attained longer for a higher $T_{m\text{-}in}$. Fig 5

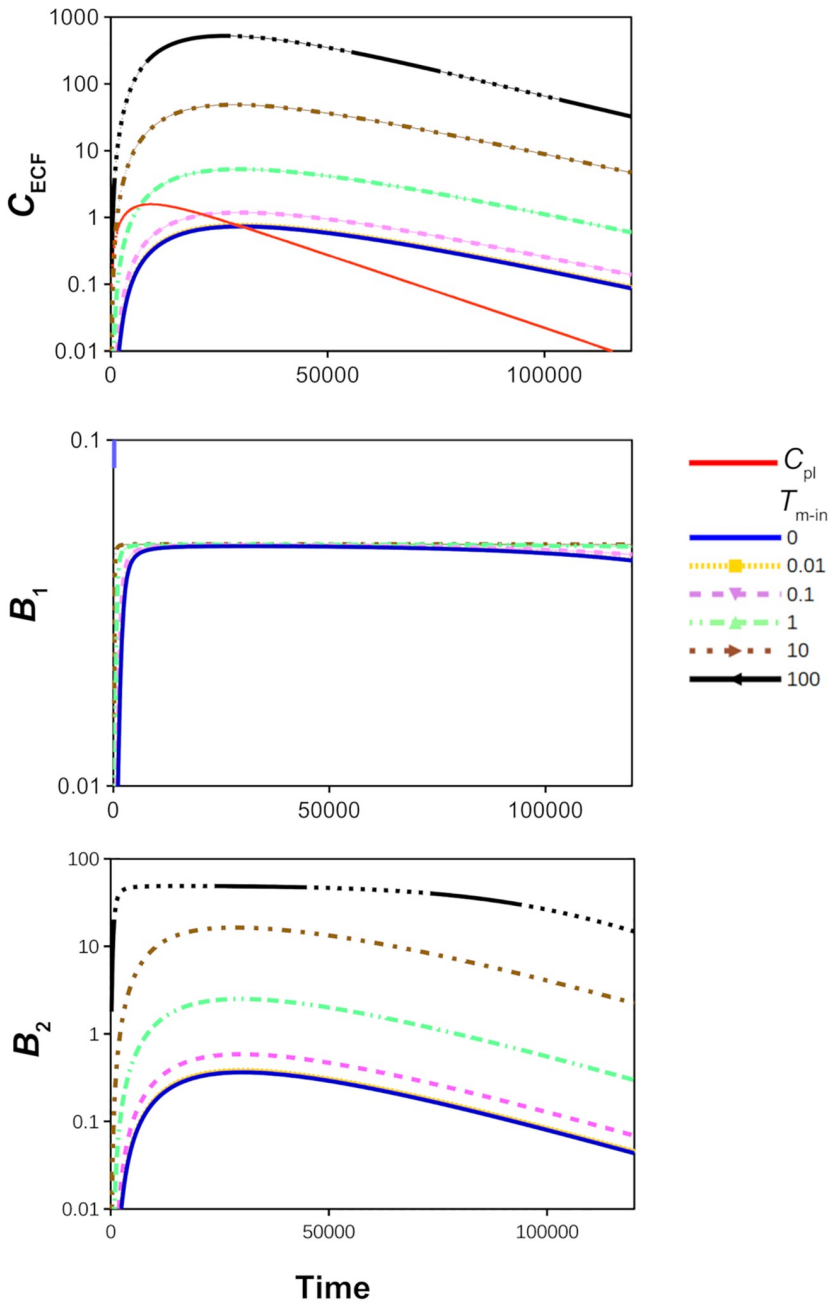

Fig 5. The effect of active influx on the log concentration-time profiles of drug in the brain ECF, relative to those in the blood plasma. Top: unbound drug in the brain ECF (C_{ECF}) compared to unbound drug in the blood plasma (C_{pl}, red curve). Middle: drug bound to its target sites (B_1). Bottom: drug bound to non-specific binding sites (B_2). The value of $T_{m\text{-}in}$ is changed from 0 to $100{\cdot}10^{-7}$ μmol s^{-1}. The rest of the parameters are as in Table 2.

https://doi.org/10.1371/journal.pone.0238397.g005

(bottom) shows that higher values of $T_{m\text{-}in}$ correlate with higher values of B_2 and thus a greater occupancy of non-specific binding sites. The non-specific binding sites within the brain ECF become saturated with drug when $T_{m\text{-}in}$ is sufficiently high ($T_{m\text{-}in} = 100{\cdot}10^{-7}$ μmol s^{-1}). To evaluate the effect of active efflux on drug concentrations within the brain ECF, we repeat our simulations with T_m directed outward, i.e. with $T_{m\text{-}out} = 0\text{-}100{\cdot}10^{-7}$ μmol s^{-1} and $T_{m\text{-}in} = 0$. Fig 6

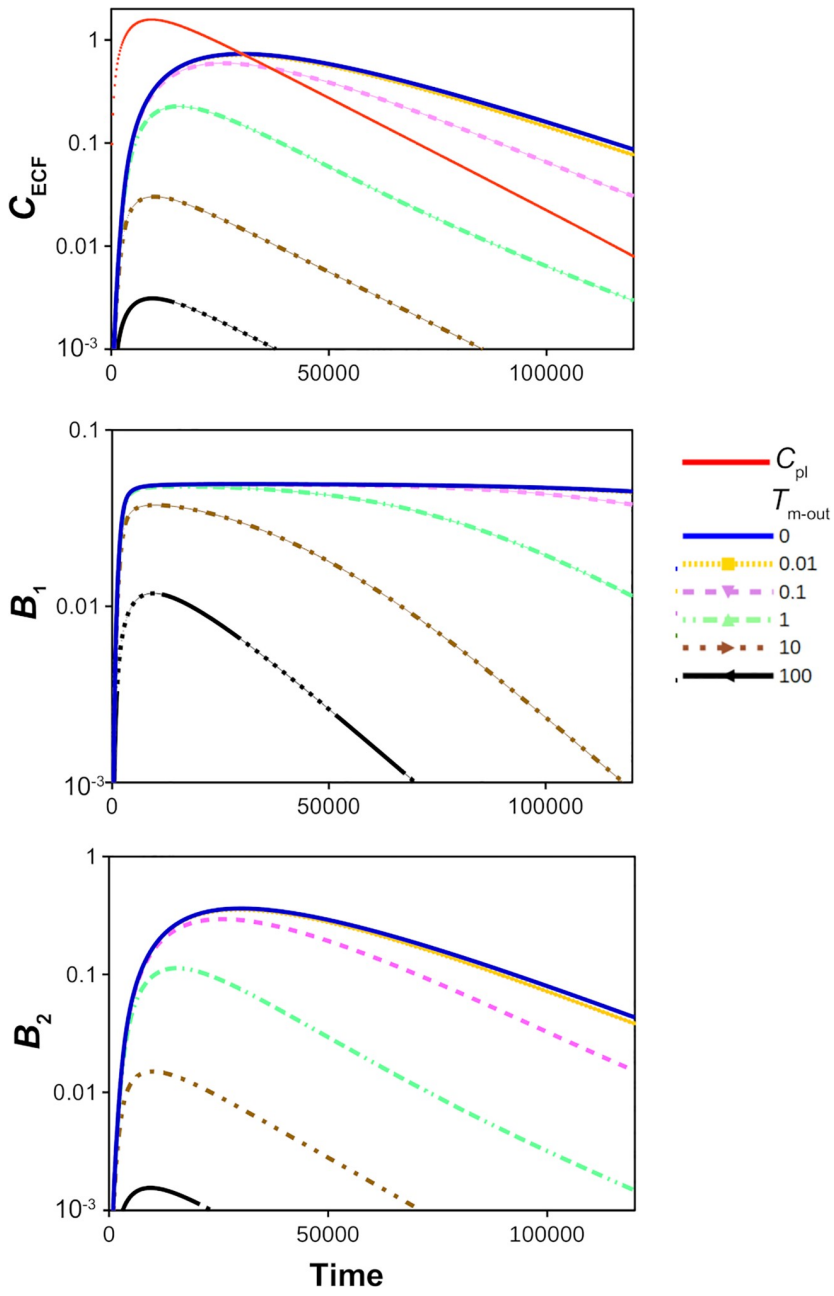

Fig 6. The effect of active efflux on the log concentration-time profiles of drug in the brain ECF, relative to those in the blood plasma. Top: unbound drug in the brain ECF (C_{ECF}) and unbound drug in the blood plasma (C_{pl}, red curve). Middle: drug bound to its target sites (B_1). Bottom: drug bound to non-specific binding sites (B_2). The value of $T_{m\text{-}out}$ is changed from 0 to $100 \cdot 10^{-7}$ μmol s^{-1}. The rest of the parameters are as in Table 2.

https://doi.org/10.1371/journal.pone.0238397.g006

(top) shows that C_{ECF} decreases faster for higher values of $T_{m\text{-}out}$, corresponding to more active efflux. Fig 6 (middle) reveals that $T_{m\text{-}out}$ affects the time during which specific binding sites are saturated: the time at which B_1 attains 90% max(B_1) is smaller for a high value of $T_{m\text{-}out}$. For sufficiently high values of $T_{m\text{-}out}$, the binding sites do not become saturated. Fig 6 (bottom) shows that B_2 is similarly affected by active efflux as C_{ECF}.

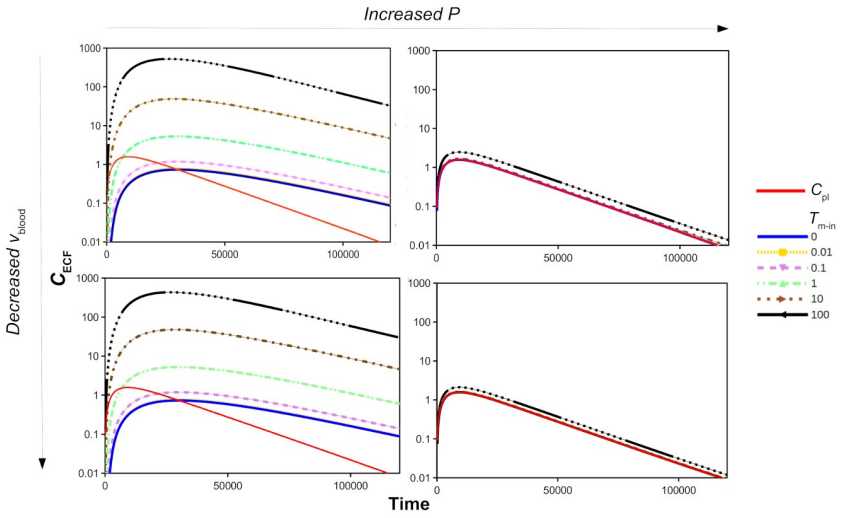

Fig 7. The log concentration-time profiles of unbound drug in brain ECF (C_{ECF}) with 1000x increased permeability P (left to right, $0.1{\cdot}10^{-7}$ m s^{-1} to $100{\cdot}10^{-7}$ m s^{-1}) or 10x decreased flow v_{ECF} (top to bottom, $5{\cdot}10^{-4}$m s^{-1} to $0.5{\cdot}10^{-4}$ m s^{-1}) in the presence of active influx compared to the concentration of unbound drug in the blood plasma (C_{pl}, red curve). The value of of $T_{m\text{-}in}$ is changed from 0 to $100{\cdot}10^{-7}$ μmol s^{-1}, as depicted by various colours. The rest of the parameters are as in Table 2.

https://doi.org/10.1371/journal.pone.0238397.g007

3.3 The effect of the brain capillary blood flow velocity in the presence of active transport

In section 3.1 we have shown that both the passive BBB permeability, P, and the brain capillary blood flow velocity, v_{blood}, affect dug brain ECF PK in the absence of active transport. Here, we study how P and v_{blood} combined with active transport affect drug PK within the brain ECF. Fig 7 shows the log plot of C_{ECF} for $v_{blood} = 5{\cdot}10^{-4}$ m s^{-1} (top) and $v_{blood} = 0.5{\cdot}10^{-4}$ m s^{-1} (bottom) and for $P = 0.1{\cdot}10^{-7}$ m s^{-1} (left) and $P = 100{\cdot}10^{-7}$ m s^{-1} (right) in the presence of active influx, i.e. for various values of $T_{m\text{-}in}$ ($T_{m\text{-}out} = 0$). Note that the vertical scale is the same in all plots. Fig 7 shows how P and v_{blood} affect the impact of $T_{m\text{-}in}$ on brain ECF PK. A smaller value of v_{blood} only slightly reduces C_{ECF} when $T_{m\text{-}in}$ is sufficiently high ($T_{m\text{-}in} \geq 10{\cdot}10^{-7}$ μmol s^{-1}), see Fig 7, left. An increase in P does reduce the impact of $T_{m\text{-}in}$ on C_{ECF} substantially (Fig 7, right). When the BBB is very permeable, like for drugs that easily cross the BBB, such as phenytoin [27, 71], active influx needs to be fast to have any effect, as drug can easily pass the BBB to flow back into the blood plasma. As shown in Fig 7, right, in the presence of a high value of P, $T_{m\text{-}in}$ only (slightly) affects C_{ECF} when it is $10{\cdot}10^{-7}$ μmol s^{-1} or higher.

Fig 8 shows the log profiles of C_{ECF} for $v_{blood} = 5{\cdot}10^{-4}$ m s^{-1} (top) and $v_{blood} = 0.5{\cdot}10^{-4}$ m s^{-1} (bottom) and for $P = 0.1{\cdot}10^{-7}$ m s^{-1} (left) and $P = 100{\cdot}10^{-7}$ m s^{-1} (right) in the presence of active efflux, i.e. for various values of $T_{m\text{-}out}$ ($T_{m\text{-}in} = 0$). Fig 8 reveals that v_{blood} does not affect the impact of $T_{m\text{-}out}$ on C_{ECF}. This is expected, as v_{blood} mainly affects C_{pl}, while active efflux depends on C_{ECF}. The passive permeability P does affect the impact of $T_{m\text{-}out}$ on C_{ECF}. If P is high, drug can easily flow across the BBB back into the brain ECF, following the concentration gradient between the blood plasma and the brain ECF, thereby countering the effect of $T_{m\text{-}out}$. Fig 8 (top right) shows that for a high P, C_{ECF} is only affected by $T_{m\text{-}out}$ when its value is higher than $10{\cdot}10^{-7}$ μmol s^{-1}. The values of C_{ECF} in the presence of active efflux and a high passive BBB permeability, P, are unaffected by v_{blood} (Fig 8, right).

Next, we study how the drug distribution within the 3D brain unit is affected by v_{blood}, P, $T_{m\text{-}in}$ and $T_{m\text{-}out}$. Fig 9 shows cross-sections (for $y = \frac{1}{2}y_r$ and $z = 0$) of the 3D brain unit at

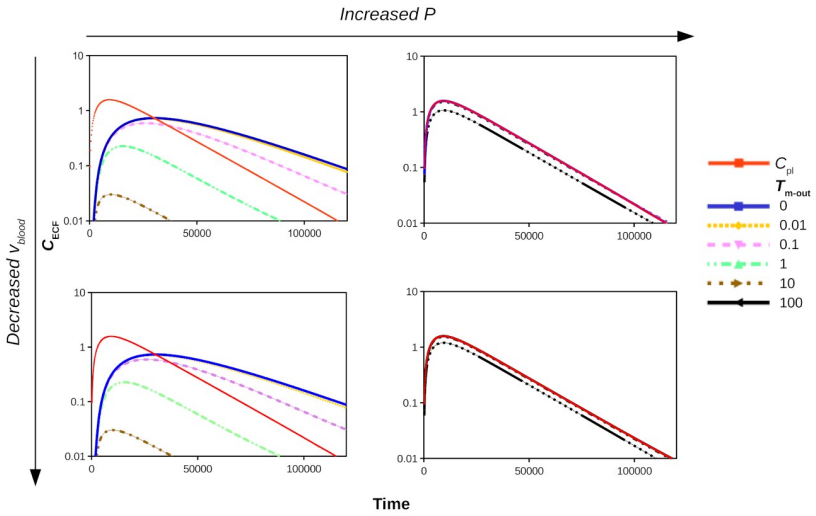

Fig 8. The PK on log-scale of unbound drug in brain ECF (C_{ECF}) with 1000x increased permeability *P* (left to right, $0.1{\cdot}10^{-7}$ m s^{-1} to $100{\cdot}10^{-7}$ m s^{-1}) and 10x decreased blood flow velocity v_{blood} (top to bottom, $5{\cdot}10^{-4}$ m s^{-1} to $0.5{\cdot}10^{-4}$ m s^{-1}) in the presence of active efflux compared to the concentration of unbound drug in the blood plasma (C_{pl}, red curve). The value of $T_{m\text{-}out}$ is changed from 0 to $100{\cdot}10^{-7}$ μmol s^{-1}, as indicated by the different colours. The rest of the parameters are as in Table 2.

https://doi.org/10.1371/journal.pone.0238397.g008

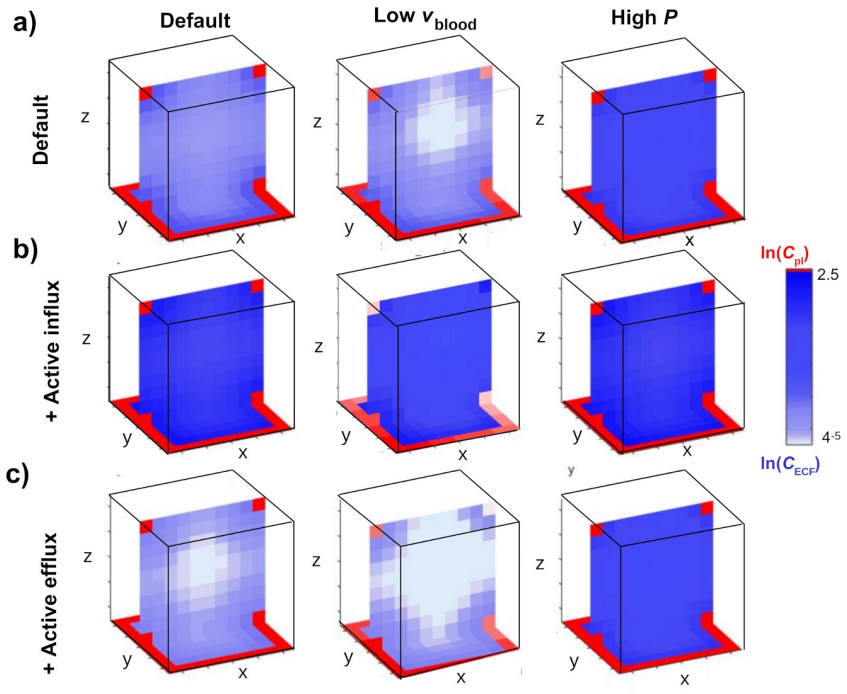

Fig 9. The distribution profiles at cross-sections (at $y = \frac{1}{2}y_r$) of the 3D brain unit at t = 5 of unbound drug in brain ECF with lower brain capillary blood flow velocity (v_{blood} = $0.5{\cdot}10^{-4}$ m s^{-1}, middle column), higher passive BBB permeability (*P* = $100{\cdot}10^{-7}$ m s^{-1}, right column), presence of active influx (middle row, $T_{m\text{-}in}$ = $1{\cdot}10^{-7}$ μmol s^{-1}) and presence of active efflux (bottom row, $T_{m\text{-}out}$ = $1{\cdot}10^{-7}$ μmol s^{-1}) at t = 5. Parameters are as in Table 2.

https://doi.org/10.1371/journal.pone.0238397.g009

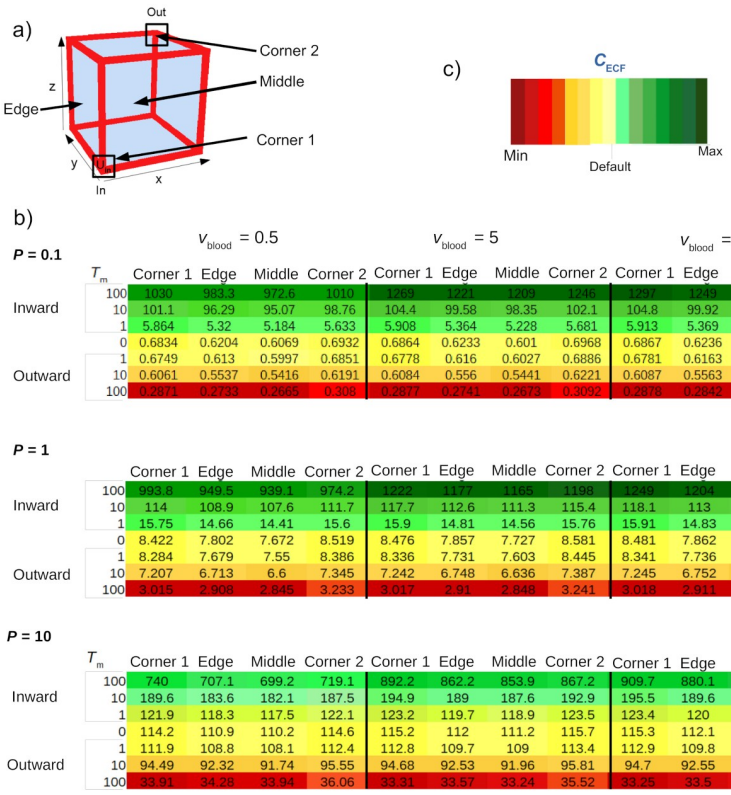

P = 0.1

T_m	Corner 1	Edge	Middle	Corner 2	Corner 1	Edge	Middle	Corner 2	Corner 1	Edge	Middle	Corner 2
Inward 100	1030	983.3	972.6	1010	1269	1221	1209	1246	1297	1249	1237	1273
10	101.1	96.29	95.07	98.76	104.4	99.58	98.35	102.1	104.8	99.92	98.68	102.4
1	5.864	5.32	5.184	5.633	5.908	5.364	5.228	5.681	5.913	5.369	5.233	5.685
0	0.6834	0.6204	0.6069	0.6932	0.6864	0.6233	0.601	0.6968	0.6867	0.6236	0.6102	0.6972
Outward 1	0.6749	0.613	0.5997	0.6851	0.6778	0.616	0.6027	0.6886	0.6781	0.6163	0.603	0.689
10	0.6061	0.5537	0.5416	0.6191	0.6084	0.556	0.5441	0.6221	0.6087	0.5563	0.5443	0.6224
100	0.2871	0.2733	0.2665	0.308	0.2877	0.2741	0.2673	0.3092	0.2878	0.2842	0.2674	0.3094

P = 1

	Corner 1	Edge	Middle	Corner 2	Corner 1	Edge	Middle	Corner 2	Corner 1	Edge	Middle	Corner 2
Inward 100	993.8	949.5	939.1	974.2	1222	1177	1165	1198	1249	1204	1192	1225
10	114	108.9	107.6	111.7	117.7	112.6	111.3	115.4	118.1	113	111.7	115.8
1	15.75	14.66	14.41	15.6	15.9	14.81	14.56	15.76	15.91	14.83	14.58	15.77
0	8.422	7.802	7.672	8.519	8.476	7.857	7.727	8.581	8.481	7.862	7.733	8.587
Outward 1	8.284	7.679	7.55	8.386	8.336	7.731	7.603	8.445	8.341	7.736	7.609	8.451
10	7.207	6.713	6.6	7.345	7.242	6.748	6.636	7.387	7.245	6.752	6.64	7.391
100	3.015	2.908	2.845	3.233	3.017	2.91	2.848	3.241	3.018	2.911	2.849	3.242

P = 10

T_m	Corner 1	Edge	Middle	Corner 2	Corner 1	Edge	Middle	Corner 2	Corner 1	Edge	Middle	Corner 2
Inward 100	740	707.1	699.2	719.1	892.2	862.2	853.9	867.2	909.7	880.1	871.7	884.3
10	189.6	183.6	182.1	187.5	194.9	189	187.6	192.9	195.5	189.6	188.1	193.4
1	121.9	118.3	117.5	122.1	123.2	119.7	118.9	123.5	123.4	120	119.1	123.6
0	114.2	110.9	110.2	114.6	115.2	112	111.2	115.7	115.3	112.1	111.4	115.8
Outward 1	111.9	108.8	108.1	112.4	112.8	109.7	109	113.4	112.9	109.8	109.1	113.5
10	94.49	92.32	91.74	95.55	94.68	92.53	91.96	95.81	94.7	92.55	91.98	95.84
100	33.91	34.28	33.94	36.06	33.31	33.57	33.24	35.52	33.25	33.5	33.17	35.47

Fig 10. Values of C_{ECF} (10^{-3} μ mol L^{-1}) at several locations within the brain unit for different values of P and v_{blood} at t = 500. a) Locations within the 3D brain unit. Corner 1: (x,y,z) = (r,r,r), Corner 2: (x,y,z) = (x_r-r,y_r-r,z_r-r), Edge: (x,y,z) = (0, $\frac{y_r}{2}$,$\frac{z_r}{2}$), Middle: (x,y,z) = ($\frac{x_r}{2}$,$\frac{y_r}{2}$,$\frac{z_r}{2}$). b) Values of C_{ECF} are shown for a low ($P = 0.01 \cdot 10^{-8}$ m s^{-1}), default ($P = 0.1 \cdot 10^{-8}$ m s^{-1}) and high ($P = 1 \cdot 10^{-8}$ m s^{-1}) value of P in the top, middle and bottom table, respectively. Within each table, concentrations are given for several values of v_{blood} ($v_{blood} = 0.5 \cdot 10^{-4}$ m s^{-1}, $v_{blood} = 5 \cdot 10^{-4}$ m s^{-1} and $v_{blood} = 50 \cdot 10^{-4}$ m s^{-1}, left to right), $T_{m\text{-}in}$ ($T_{m\text{-}in} = 0$, $T_{m\text{-}in} = 1 \cdot 10^{-7}$ μmol s^{-1}, $T_{m\text{-}in} = 10 \cdot 10^{-7}$ μmol s^{-1} and $T_{m\text{-}in} = 100 \cdot 10^{-7}$ μmol s^{-1}) and $T_{m\text{-}out}$ ($T_{m\text{-}out} = 0$, $T_{m\text{-}out} = 1 \cdot 10^{-7}$ μmol s^{-1}, $T_{m\text{-}out} = 10 \cdot 10^{-7}$ μmol s^{-1} and $T_{m\text{-}out} = 100 \cdot 10^{-7}$ μmol s^{-1}) at different locations. When $T_{m\text{-}in}$ is changed, $T_{m\text{-}out} = 0$ and vice versa. c) Colour legend. In each table, colours are relative to the value of C_{ECF} in the middle of the unit in the absence of active transport for $v_{blood} = 5 \cdot 10^{-4}$ m s^{-1}, of which the colour is denoted by "Default". The intensity of green corresponds to the extent of increase, and the intensity of red corresponds to the extent of decrease of C_{ECF} compared to the default. Other parameters are as in Table 2.

https://doi.org/10.1371/journal.pone.0238397.g010

t = 5, in which the distribution of C_{pl} and C_{ECF} is plotted. The values of C_{pl} and C_{ECF} are represented by shades of red and blue, respectively, where darker shades indicate higher concentrations. In Fig 9a (left) we give a plot for a default P and v_{blood} (Fig 9a, left). Then, we decrease v_{blood} (Fig 9a, middle) or increase P (Fig 9a, right). For a lower v_{blood}, relative differences of C_{pl} over space increase (Fig 9a, middle).

Additionally, due to the decrease in C_{pl}, local differences in C_{ECF} become more apparent. A larger value of P results in an increased exchange of drug between the blood plasma and the brain ECF, such that C_{ECF} becomes higher (Fig 9a, right).

Fig 9b shows that the presence of active influx ($T_{m\text{-}in} = 1 \cdot 10^{-7}$ μmol s^{-1}) increases C_{ECF}. As a consequence, local differences within U_{ECF} become relatively small. With a low value of v_{blood}, local differences in U_{pl} become apparent (Fig 9b, middle). Finally, Fig 9c shows that with active efflux, C_{ECF} becomes smaller than when no active efflux is present, except for when P is high and more pronounced.

Values of C_{ECF} are given in the table in Fig 10c in order to show the differences within the 3D brain unit more clearly. There, values of C_{ECF} are given for four different locations within

the 3D brain unit for several values of v_{blood} and P and t = 500. The table again (as in Figs 7, 8 and 9) shows that v_{blood} and P affect the impact of $T_{m\text{-}in}$ and $T_{m\text{-}out}$ on C_{ECF}. It provides additional information on the distribution of C_{ECF} within the 3D brain unit. In general, C_{ECF} is higher in the corners relative to the edge and middle within the 3D brain unit. The extent of these local concentration differences depends on the values of $T_{m\text{-}in}$ and $T_{m\text{-}out}$. The differences are largest when $T_{m\text{-}out} = 1{\cdot}10^{-7}$ μmol s^{-1}, depicted in the lowest line of each sub-table. There, C_{ECF} in corner 2 is higher than in corner 1. In addition, in the presence of active influx, the values of C_{ECF} are lower in corner 2 than in corner 1. Again, the extent of this difference depends on the value of $T_{m\text{-}in}$.

4 Discussion

We have developed a mathematical model that describes the local distribution of a drug within a 3D brain unit as an extension of our earlier 2D proof-of-concept model [31]. The 3D brain unit is represented as a cube. This new model provides an important step towards more realistic features of the brain. The 3D representation allows for the brain ECF to be represented as a continuous medium. The brain capillary blood flow and active transport across the BBB have been explicitly incorporated. This enables us to more realistically predict the impact of the interplay of cerebral blood flow, BBB characteristics, brain ECF diffusion, brain ECF bulk flow and brain (target) binding on drug distribution within the brain. Altogether our model allows the study of the effect of a large amount of parameters values (summarized in Table 1) on drug distribution within the 3D brain unit.

The current modelling work is based on certain assumptions (Assumptions 1 and 2). We will shortly discuss their probability and impact (see [72]) below. Assumptions 1(i), 1(ii), 1(iv), 1(v), 2(i), 2(iii), 2(v), 2(vi) and 2(viii) are based on actual physiological processes, adapted to the simplified geometry of the 3D brain unit. Therefore, these assumptions are unlikely to be violated, but the impact of violation would be high on the results of the simulations. Assumptions 1(iii) and 1(vi) are known to be more complex in real, but are expected to have a small impact when violated. Assumption 1(vii) is not violated for drugs that do not bind plasma proteins. However, for drugs that do bind plasma proteins, the assumption is likely violated with an impact to be investigated in future work. In similar fashion, assumptions 2(ii), 2(iv) and 2 (vii) are not violated for drugs that do not cross cells, but it is likely that for drugs that do, they are violated with an impact to be investigated in future work.

In the present work, we have investigated the properties of the 3D brain unit with a sensitivity analysis and thus looking at hypothetical compounds. The advantage of studying the model in this way is that it allows us to investigate a wider range of parameter values than an existing compound would have allowed. Moreover, the hypothetical compound has parameter values that are within and on the extremes of the reported physiological ranges and we therefore believe that it is an accurate representation of reality. The study has focused on the effect of the newly implemented brain properties on brain ECF concentrations a drug within the brain. It is shown that the brain capillary blood flow velocity and the passive BBB permeability affect the concentration of a drug within the brain, and, as anticipated [73, 74] that a low brain capillary blood flow velocity affects the short-term, but not the long-term concentration-time profiles of C_{pl} and C_{ECF} (Figs 3 and 4). In addition to the confirmation of these earlier reported results, our model enables the study of the effects of BBB permeability in conjunction with other factors, like active BBB transport, on brain ECF PK. It was found that passive BBB permeability has a high impact on brain ECF PK, even when drug is actively transported across the BBB. Moreover, the BBB permeability and, in smaller extent, the brain capillary blood flow velocity affect the impact of active influx on drug PK within the brain ECF (Figs 7 and 8).

Interestingly, the brain capillary blood flow velocity, passive BBB permeability and active transport do not only affect the concentration of drug within the brain ECF, but also its distribution within the brain ECF (Figs 9 and 10). The local differences observed within the 3D brain unit exist on a relatively small time-scale. It is anticipated that in certain cases, like those of high drug-target binding or active transport, these differences may also exist on a larger time-scale, but this requires further investigation.

To ensure the quality of a mathematical model, the model predictions are ideally compared to experimental data. Validation of the presented model however, describing spatial drug distribution within the brain ECF, is not straightforward. As experimental data on spatial drug distribution within brain ECF are not yet available on the level of detail as predicted by our model, we show results that are new. The results of our simulation are therefore a hypothesis and serve as a lead for experiments. For the present work, it is already possible to validate parts of the model. For example, in the current manuscript, we have compared our results on the effect of brain capillary blood flow on BBB influx with the well-established Renkin-Crone equation. The results were shown to agree, which supports our hypothesis that our basic description of blood plasma PK is realistic. Ideally, a thorough interplay between theoretical and experimental work is developed in future, leading to a gain in knowledge in spatial drug distribution on the most efficient way possible.

Taken together, the current 3D brain unit model shows the impact of drug-specific and brain-specific parameters on drug distribution within the brain ECF. The added value is that all these factors can now be studied *in conjunction* to understand the interdependencies of multiple brain parameter values and drug properties, as was shown in this work. This makes this single 3D brain unit model suitable for the next step, which is to mount up multiple units to represent a larger volume of brain tissue, in which the brain tissue properties for each unit can be defined independently. With the establishment of the current 3D brain unit model, we are now ready to incorporate intra-extracellular exchange and drug binding to intracellular binding sites in future modelling work. As the current model is in 3D, the units can be built up, and drug distribution within the brain ECF can be described, in all possible directions. The units may be given different systemic properties (such as the BBB permeability or drug target concentration), to represent the heterogeneity of the brain in a 3D manner.

Supporting information

S1 Appendix. Nondimensionalization of the model.
(PDF)

S2 Appendix. The effect of paracellular permeability on PK within the brain ECF.
(PDF)

S3 Appendix. The Renkin-Crone equation and the 3D brain unit model. [67, 68, 75].
(PDF)

Author Contributions

Conceptualization: Esmée Vendel, Vivi Rottschäfer, Elizabeth C. M. de Lange.

Investigation: Esmée Vendel, Vivi Rottschäfer, Elizabeth C. M. de Lange.

Methodology: Esmée Vendel, Vivi Rottschäfer, Elizabeth C. M. de Lange.

Writing – original draft: Esmée Vendel, Vivi Rottschäfer, Elizabeth C. M. de Lange.

Writing – review & editing: Esmée Vendel, Vivi Rottschäfer, Elizabeth C. M. de Lange.

References

1. Vendel E, Rottschäfer V, de Lange ECM. The need for mathematical modelling of spatial drug distribution within the brain. Fluids and Barriers of the CNS. 2019; 16(12). https://doi.org/10.1186/s12987-019-0133-x PMID: 31092261
2. Summerfield SG, Stevens AJ, Cutler L, del Carmen Osuna M, Hammond B, Tang SP, et al. Improving the in Vitro Prediction of in Vivo Central Nervous System Penetration: Integrating Permeability, P-glycoprotein Efflux, and Free Fractions in Blood and Brain. The Journal of Pharmacology and Experimental Therapeutics. 2006; 316(3):1282–1290. https://doi.org/10.1124/jpet.105.092916 PMID: 16330496
3. Summerfield SG, Lucas AJ, Porter RA, Jeffrey P, Gunn RN, Read KR, et al. Toward an improved prediction of human in vivo brain penetration. Xenobiotica. 2008; 38(12):1518–1535. https://doi.org/10.1080/00498250802499459 PMID: 18979396
4. Tsuji A. Small molecular drug transfer across the blood-brain barrier via carrier-mediated transport systems. NeuroRx: the journal of the American Society for Experimental NeuroTherapeutics. 2005; 2 (1):54–62. https://doi.org/10.1602/neurorx.2.1.54 PMID: 15717057
5. van Bree JB, de Boer AG, Danhof M, Ginsel LA, Breimer DD. Characterization of an "in vitro" blood-brain barrier: effects of molecular size and lipophilicity on cerebrovascular endothelial transport rates of drugs. Journal of Pharmacology and Experimental Therapeutics. 1988; 247(3):1233–1239. PMID: 3204515
6. Hammarlund-Udenaes M, Paalzow LK, de Lange ECM. Drug Equilibration Across the Blood-Brain Barrier-Pharmacokinetic Considerations Based on the Microdialysis Method. Pharmaceutical Research. 1997; 14(2):128–134. https://doi.org/10.1023/A:1012080106490 PMID: 9090698
7. Waterhouse RN. Determination of lipophilicity and its use as a predictor of blood–brain barrier penetration of molecular imaging agents. Molecular Imaging & Biology. 2003; 5(6):376–389. https://doi.org/10.1016/j.mibio.2003.09.014 PMID: 14667492
8. Löscher W, Potschka H. Role of drug efflux transporters in the brain for drug disposition and treatment of brain diseases. Progress in Neurobiology. 2005; 76(1):22–76. https://doi.org/10.1016/j.pneurobio.2005.04.006 PMID: 16011870
9. Syvänen S, Xie R, Sahin S, Hammarlund-Udenaes M. Pharmacokinetic consequences of active drug efflux at the blood-brain barrier. Pharmaceutical Research. 2006; 23(4):705–717. https://doi.org/10.1007/s11095-006-9780-0 PMID: 16575498
10. Watanabe T, Kusuhara H, Maeda K, Shitara Y, Sugiyama Y. Physiologically based pharmacokinetic modeling to predict transporter-mediated clearance and distribution of pravastatin in humans. Journal of Pharmacology and Experimental Therapeutics. 2009; 328(2):652–662. https://doi.org/10.1124/jpet.108.146647 PMID: 19001154
11. Nicholson C, Phillips JM. Ion diffusion modified by tortuosity and volume fraction in the extracellular microenvironment of the rat cerebellum. The Journal of Physiology. 1981; 321:225. https://doi.org/10.1113/jphysiol.1981.sp013981 PMID: 7338810
12. Nicholson C. Diffusion and related transport mechanisms in brain tissue. Reports on Progress in Physics. 2001; 64(7):815. https://doi.org/10.1088/0034-4885/64/7/202
13. Wang Y, Welty DR. The simultaneous estimation of the influx and efflux blood-brain barrier permeabilities of gabapentin using a microdialysis-pharmacokinetic approach. Pharmaceutical Research. 1996; 13(3):398–403. https://doi.org/10.1023/A:1016092525901 PMID: 8692732
14. Liu X, Vilenski O, Kwan J, Apparsundaram S, Weiker R. Unbound brain concentration determines receptor occupancy: a correlation of drug concentration and brain serotonin and dopamine reuptake transporter occupancy for eighteen compounds in rats. Drug Metabolism and Disposition. 2009.
15. Vauquelin G. On the 'micro'-pharmacodynamic and pharmacokinetic mechanisms that contribute to long-lasting drug action. Expert Opinion on Drug Discovery. 2015; 10(10):1085–1098. https://doi.org/10.1517/17460441.2015.1067196 PMID: 26165720
16. de Witte WEA, Danhof M, van der Graaf PH, de Lange ECM. In vivo Target Residence Time and Kinetic Selectivity: The Association Rate Constant as Determinant. Trends in Pharmacological Sciences. 2016; 37(10):831–842. https://doi.org/10.1016/j.tips.2016.06.008 PMID: 27394919
17. Pan AC, Borhani DW, Dror RO, Shaw DE. Molecular determinants of drug-receptor binding kinetics. Drug Discovery Today. 2013; 18(13-14):667–673. https://doi.org/10.1016/j.drudis.2013.02.007 PMID: 23454741
18. Collins JM, Dedrick RL. Distributed model for drug delivery to CSF and brain tissue. American Journal of Physiology-Regulatory, Integrative and Comparative Physiology. 1983; 245(3):R303–R310. https://doi.org/10.1152/ajpregu.1983.245.3.R303 PMID: 6614201
19. de Lange ECM, Ravenstijn PGM, Groenendaal D, van Steeg TJ. Toward the prediction of CNS drug-effect profiles in physiological and pathological conditions using microdialysis and mechanism-based

pharmacokinetic-pharmacodynamic modeling. The AAPS journal. 2005; 7(3):E532–E543. https://doi.org/10.1208/aapsj070354 PMID: 16353931

20. Ball K, Bouzom F, Scherrmann JM, Walther B, DeclÃ¨ves X. A Physiologically Based Modeling Strategy during Preclinical CNS Drug Development. Molecular Pharmaceutics. 2014; 11:836–848. https://doi.org/10.1021/mp400533q PMID: 24446829

21. Nhan T, Burgess A, Lilge L, Hynynen K. Modeling localized delivery of Doxorubicin to the brain following focused ultrasound enhanced blood-brain barrier permeability. Physics in Medicine & Biology. 2014; 59:5987–6004. https://doi.org/10.1088/0031-9155/59/20/5987 PMID: 25230100

22. Calvetti D, Cheng Y, Somersalo E. A spatially distributed computational model of brain cellular metabolism. Journal of Theoretical Biology. 2015; 376:48–65. https://doi.org/10.1016/j.jtbi.2015.03.037 PMID: 25863266

23. Ehlers W, Wagner A. Multi-component modelling of human brain tissue: a contribution to the constitutive and computational description of deformation, flow and diffusion processes with application to the invasive drug-delivery problem. Computer Methods in Biomechanics and Biomedical Engineering. 2015; 18(8):861–879. https://doi.org/10.1080/10255842.2013.853754 PMID: 24261340

24. Trapa PE, Belova E, Liras JL, Scott DO, Steyn SJ. Insights From an Integrated Physiologically Based Pharmacokinetic Model for Brain Penetration. Journal of Pharmaceutical Sciences. 2016; 105(2):965–971. https://doi.org/10.1016/j.xphs.2015.12.005 PMID: 26869440

25. Gaohua L, Neuhoff S, Johnson TN, Rostami-Hodjegan A, Jamei M. Development of a permeability-limited model of the human brain and cerebrospinal fluid (CSF) to integrate known physiological and biological knowledge: Estimating time varying CSF drug concentrations and their variability using in vitro data. Drug Metabolism and Pharmacokinetics. 2016; 31(3):224–233. https://doi.org/10.1016/j.dmpk.2016.03.005 PMID: 27236639

26. Zhan W, Arifin DY, Lee TKY, Wang CH. Mathematical Modelling of Convection Enhanced Delivery of Carmustine and Paclitaxel for Brain Tumour Therapy. Pharm Res. 2017; 34:860–873. https://doi.org/10.1007/s11095-017-2114-6 PMID: 28155074

27. Yamamoto Y, Danhof M, de Lange ECM. Microdialysis: the key to physiologically based model prediction of human CNS target site concentrations. The AAPS journal. 2017; 19(4):891–909. https://doi.org/10.1208/s12248-017-0080-x PMID: 28281195

28. Yamamoto Y, Välitalo PA, Wong YC, Huntjes DR, Proost JH, Vermeulen A, et al. Prediction of human CNS pharmacokinetics using a physiologically-based pharmacokinetic modeling approach. European Journal of Pharmaceutical Sciences. 2018; 112:168–179. https://doi.org/10.1016/j.ejps.2017.11.011 PMID: 29133240

29. Kalvass JC, Maurer TS. Influence of non-specific brain and plasma binding on CNS exposure: implications for rational drug discovery. Biopharmaceutics & Drug Disposition. 2002; 23(8):327–338. https://doi.org/10.1002/bdd.325 PMID: 12415573

30. Gustafsson S, Sehlin D, Lampa E, Hammarlund-Udenaes M, Loryan I. Heterogeneous drug tissue binding in brain regions of rats, Alzheimer's patients and controls: impact on translational drug development. Scientific reports. 2019; 9(1):5308. https://doi.org/10.1038/s41598-019-41828-4 PMID: 30926941

31. Vendel E, Rottschäfer V, de Lange ECM. Improving the Prediction of Local Brain Distribution Profiles with a New Mathematical Model. Bulletin for Mathematical Biology, Special Issue on "Mathematics to Support Drug Discovery and Development". 2018; p. 1–31.

32. Rowland M, Tozer TN. Clinical Pharmacokinetics and Pharmacodynamics. Lippincott Williams and Wilkins Philadelphia; 2005.

33. Roanes-Lozano E, González-Bermejo A, Roanes-Macías E, Cabezas J. An application of computer algebra to pharmacokinetics: the Bateman equation. SIAM review. 2006; 48(1):133–146. https://doi.org/10.1137/050634074

34. Jucker M, Bättig K, Meier-Ruge W. Effects of aging and vincamine derivatives on pericapillary microenvironment: stereological characterization of the cerebral capillary network. Neurobiology of Aging. 1990; 11(1):39–46. https://doi.org/10.1016/0197-4580(90)90060-D PMID: 2325815

35. Schlageter KE, Molnar P, Lapin GD, Groothuis DR. Microvessel organization and structure in experimental brain tumors: microvessel populations with distinctive structural and functional properties. Microvascular Research. 1999; 58(3):312–328. https://doi.org/10.1006/mvre.1999.2188 PMID: 10527772

36. Pardridge WM. The blood-brain barrier: bottleneck in brain drug development. NeuroRx: the Journal of the American Society for Experimental NeuroTherapeutics. 2005; 2(1):3–14. https://doi.org/10.1602/neurorx.2.1.3

37. Tata DA, Anderson BJ. A new method for the investigation of capillary structure. Journal of Neuroscience Methods. 2002; 113(2):199–206. https://doi.org/10.1016/S0165-0270(01)00494-0 PMID: 11772441

38. McGinty S, Pontrelli G. On the role of specific drug binding in modelling arterial eluting stents. Journal of Mathematical Chemistry. 2016; 54(4):967–976. https://doi.org/10.1007/s10910-016-0618-7

39. Tzafriri AR, Groothuis A, Price GS, Edelman ER. Stent elution rate determines drug deposition and receptor-mediated effects. Journal of Controlled Release. 2012; 161(3):918–926. https://doi.org/10.1016/j.jconrel.2012.05.039 PMID: 22642931

40. Tasso L, Bettoni CC, Costa TD. Pharmacokinetic plasma profile and bioavailability evaluation of gatifloxacin in rats. Latin American Journal of Pharmacy. 2008; 27(2):270–273.

41. Karbowski J. Scaling of brain metabolism and blood flow in relation to capillary and neural scaling. PLOS ONE. 2011; 6(10). https://doi.org/10.1371/journal.pone.0026709 PMID: 22053202

42. Nicholson C, Chen KC, Hrabětová S, Tao L. Diffusion of molecules in brain extracellular space: theory and experiment. Progress in Brain Research. 2000; 125:129–154. https://doi.org/10.1016/S0079-6123(00)25007-3 PMID: 11098654

43. Nicholson C, Kamali-Zare P, Tao L. Brain Extracellular Space as a Diffusion Barrier. Computing and Visualization in Science. 2011; 14(7):309–325. https://doi.org/10.1007/s00791-012-0185-9 PMID: 23172993

44. Saltzman WM. Interstitial transport in the brain: principles for local drug delivery. In: Transport Phenomena in Biomedical Engineering. CRC Press; 2012. p. 158–171.

45. Hladky SB, Barrand MA. Mechanisms of fluid movement into, through and out of the brain: evaluation of the evidence. Fluids and Barriers of the CNS. 2014; 11(1):1. https://doi.org/10.1186/2045-8118-11-26 PMID: 25678956

46. Wong AD, Ye M, Levy AF, Rothstein JD, Bergles DE, Searson PC. The blood-brain barrier: an engineering perspective. Frontiers in Neuroengineering. 2013; 6:7. https://doi.org/10.3389/fneng.2013.00007 PMID: 24009582

47. Lentz KA, Polli JW, Wring SA, Humphreys JE, Polli JE. Influence of passive permeability on apparent P-glycoprotein kinetics. Pharmaceutical Research. 2000; 17(12):1456–1460. https://doi.org/10.1023/A:1007692622216 PMID: 11303953

48. Hoffmann J, Fichtner I, Lemm M, Lienau P, Hess-Stumpp H, Rotgeri A, et al. Sagopilone crosses the blood–brain barrier in vivo to inhibit brain tumor growth and metastases. Neuro-oncology. 2009; 11(2):158–166. https://doi.org/10.1215/15228517-2008-072) PMID: 18780814

49. Takasato Y, Rapoport SI, Smith QR. An in situ brain perfusion technique to study cerebrovascular transport in the rat. American Journal of Physiology-Heart and Circulatory Physiology. 1984; 247(3):H484–H493. https://doi.org/10.1152/ajpheart.1984.247.3.H484 PMID: 6476141

50. Liu X, Tu M, Kelly RS, Chen C, Smith BJ. Development of a computational approach to predict blood-brain barrier permeability. Drug Metabolism and Disposition. 2004; 32(1):132–139. https://doi.org/10.1124/dmd.32.1.132 PMID: 14709630

51. Youdim KA, Qaiser MZ, Begley DJ, Rice-Evans CA, Abbott NJ. Flavonoid permeability across an in situ model of the blood–brain barrier. Free Radical Biology and Medicine. 2004; 36(5):592–604. https://doi.org/10.1016/j.freeradbiomed.2003.11.023 PMID: 14980703

52. Summerfield SG, Read K, Begley DJ, Obradovic T, Hidalgo IJ, Coggon S, et al. Central nervous system drug disposition: the relationship between in situ brain permeability and brain free fraction. The Journal of Pharmacology and Experimental Therapeutics. 2007; 322(1):205–213. https://doi.org/10.1124/jpet.107.121525 PMID: 17405866

53. Bruns RF, Daly JW, Snyder SH. Adenosine receptors in brain membranes: binding of N6-cyclohexyl [3H] adenosine and 1, 3-diethyl-8-[3H] phenylxanthine. Proceedings of the National Academy of Sciences. 1980; 77(9):5547–5551. https://doi.org/10.1073/pnas.77.9.5547 PMID: 6254090

54. Perry DC, Mullis KB, Øie S, Sadée W. Opiate antagonist receptor binding in vivo: evidence for a new receptor binding model. Brain Research. 1980; 199(1):49–61. https://doi.org/10.1016/0006-8993(80)90229-2 PMID: 6250676

55. Farde L, Eriksson L, Blomquist G, Halldin C. Kinetic analysis of central [11C] raclopride binding to D2-dopamine receptors studied by PET—a comparison to the equilibrium analysis. Journal of Cerebral Blood Flow & Metabolism. 1989; 9(5):696–708. https://doi.org/10.1038/jcbfm.1989.98 PMID: 2528555

56. Levy G. Pharmacologic target-mediated drug disposition. Clinical Pharmacology & Therapeutics. 1994; 56(3):248–252. https://doi.org/10.1038/clpt.1994.134

57. Costes N, Merlet I, Zimmer L, Lavenne F, Cinotti L, Delforge J, et al. Modeling [18F] MPPF positron emission tomography kinetics for the determination of 5-hydroxytryptamine (1A) receptor concentration with multiinjection. Journal of Cerebral Blood Flow & Metabolism. 2002; 22(6):753–765. https://doi.org/10.1097/00004647-200206000-00014 PMID: 12045674

58. Millet P, Graf C, Moulin M, Ibáñez V. SPECT quantification of benzodiazepine receptor concentration using a dual-ligand approach. Journal of Nuclear Medicine. 2006; 47(5):783–792. PMID: 16644748

59. Dahl G, Akerud T. Pharmacokinetics and the drug–target residence time concept. Drug Discovery Today. 2013; 18(15-16):697–707. https://doi.org/10.1016/j.drudis.2013.02.010 PMID: 23500610

60. Ivanov KP, Kalinina MK, Levkovich YI. Blood flow velocity in capillaries of brain and muscles and its physiological significance. Microvascular Research. 1981; 22(2):143–155. https://doi.org/10.1016/0026-2862(81)90084-4 PMID: 7321902

61. Hudetz AG, Biswal BB, Fehér G, Kampine JP. Effects of hypoxia and hypercapnia on capillary flow velocity in the rat cerebral cortex. Microvascular Research. 1997; 54(1):35–42. https://doi.org/10.1006/mvre.1997.2023 PMID: 9245642

62. Seylaz J, Charbonné R, Nanri K, Von Euw D, Borredon J, Kacem K, et al. Dynamic in vivo measurement of erythrocyte velocity and flow in capillaries and of microvessel diameter in the rat brain by confocal laser microscopy. Journal of Cerebral Blood Flow & Metabolism. 1999; 19(8):863–870. https://doi.org/10.1097/00004647-199908000-00005 PMID: 10458593

63. Hutchinson EB, Stefanovic B, Koretsky AP, Silva AC. Spatial flow-volume dissociation of the cerebral microcirculatory response to mild hypercapnia. Neuroimage. 2006; 32(2):520–530. https://doi.org/10.1016/j.neuroimage.2006.03.033 PMID: 16713717

64. Itoh Y, Suzuki N. Control of brain capillary blood flow. Journal of Cerebral Blood Flow & Metabolism. 2012; 32(7):1167–1176. https://doi.org/10.1038/jcbfm.2012.5 PMID: 22293984

65. Villringer A, Them A, Lindauer U, Einhäupl K, Dirnagl U. Capillary perfusion of the rat brain cortex. An in vivo confocal microscopy study. Circulation Research. 1994; 75(1):55–62. https://doi.org/10.1161/01.RES.75.1.55 PMID: 8013082

66. Schiesser WE, Griffiths GW. A compendium of partial differential equation models: method of lines analysis with Matlab. Cambridge University Press; 2009.

67. Renkin EM. Transport of potassium-42 from blood to tissue in isolated mammalian skeletal muscles. American Journal of Physiology-Legacy Content. 1959; 197(6):1205–1210. https://doi.org/10.1152/ajplegacy.1959.197.6.1205 PMID: 14437359

68. Crone C. The permeability of capillaries in various organs as determined by use of the 'indicator diffusion' method. Acta Physiologica. 1963; 58(4):292–305. https://doi.org/10.1111/j.1748-1716.1963.tb02652.x PMID: 14078649

69. Mikitsh JL, Chacko AM. Pathways for small molecule delivery to the central nervous system across the blood-brain barrier. Perspectives in Medicinal Chemistry. 2014; 6:11. https://doi.org/10.4137/PMC.S13384 PMID: 24963272

70. Stamatovic SM, Keep RF, Andjelkovic AV. Brain endothelial cell-cell junctions: how to "open" the blood brain barrier. Current Neuropharmacology. 2008; 6(3):179–192. https://doi.org/10.2174/157015908785777210 PMID: 19506719

71. Yamamoto Y, Välitalo PA, van den Berg DJ, Hartman R, van den Brink W, Wong YC, et al. A Generic Multi-Compartmental CNS Distribution Model Structure for 9 Drugs Allows Prediction of Human Brain Target Site Concentrations. Pharmaceutical Research. 2016; p. 1–19. https://doi.org/10.1007/s11095-016-2065-3 PMID: 27864744

72. Ooi Q, Wright, Daniel FB, Isbister GK, Duffull SB. Evaluation of assumptions underpinning pharmacometric models The AAPS journal. 2019; 21: 97 https://doi.org/10.1208/s12248-019-0366-2 PMID: 31385119

73. Banks WA. Characteristics of compounds that cross the blood-brain barrier. BMC Neurology. 2009; 9(1):S3. https://doi.org/10.1186/1471-2377-9-S1-S3 PMID: 19534732

74. Hammarlund-Udenaes M, Fridén M, Syvänen S, Gupta A. On the rate and extent of drug delivery to the brain. Pharmaceutical Research. 2008; 25(8):1737–1750. https://doi.org/10.1007/s11095-007-9502-2 PMID: 18058202

75. Pardridge WM. CSF, blood-brain barrier, and brain drug delivery. Expert Opinion on Drug Delivery. 2016; 13(7):963–975. https://doi.org/10.1517/17425247.2016.1171315 PMID: 27020469